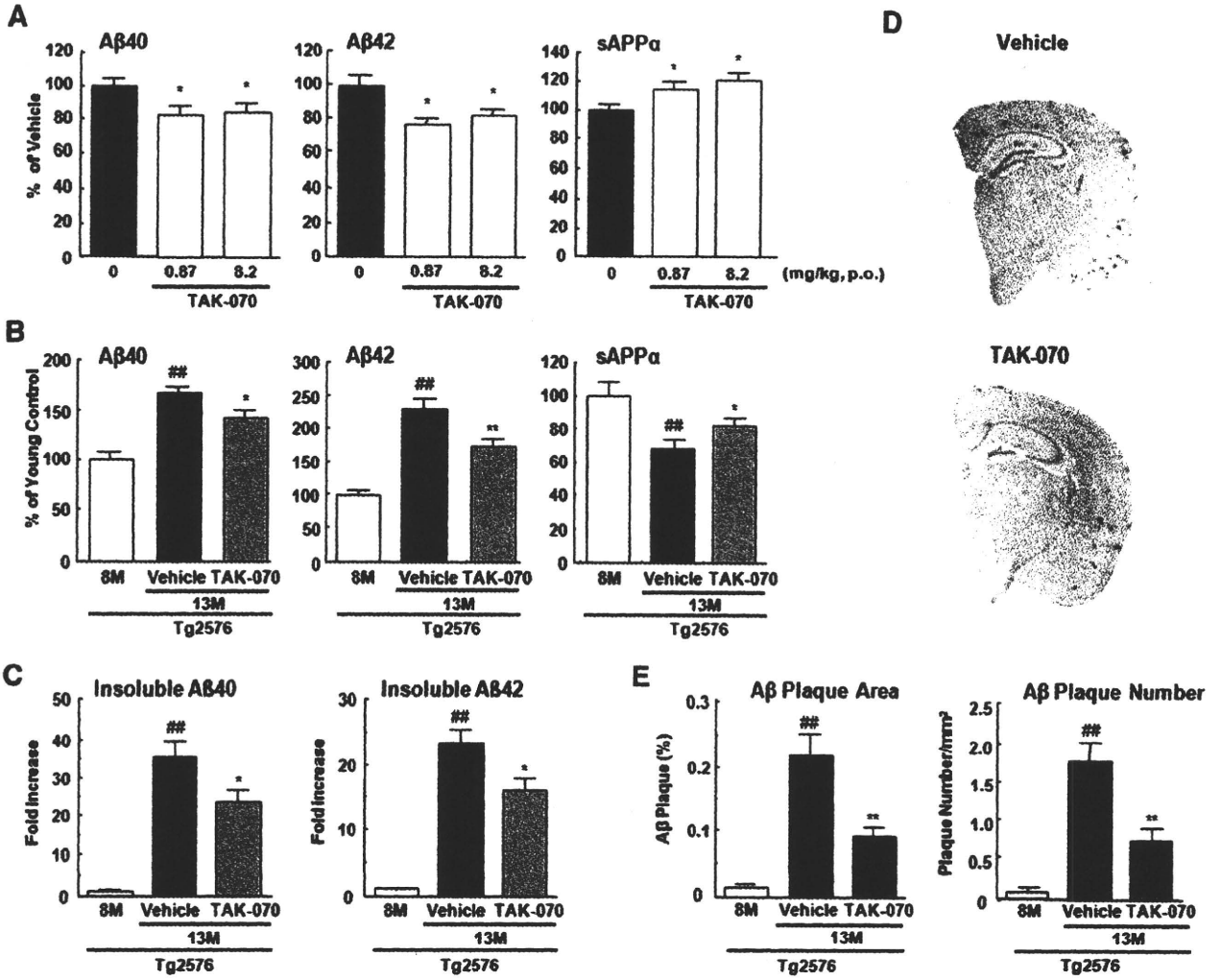

Figure 6. Effects of TAK-070 on Aβ and sAPPα levels in the brains of Tg2576 mice. ***A***, Levels of Tris-soluble $A\beta_{40}$, $A\beta_{42}$, and sAPPα in the cerebral cortices of young female Tg2576 mice after short-term administration. Values are mean percentages (±SEM) relative to levels in vehicle control ($n = 15$ for both cohorts). $^{*}p < 0.025$, versus vehicle control (one-tailed Williams test). ***B***, Levels of Tris-soluble $A\beta_{40}$, $A\beta_{42}$, and sAPPα in cerebral cortices of 13-month-old Tg2576 mice after long-term treatment. The number of 13-month-old Tg2576 mice with vehicle or TAK-070 (56 ppm, corresponding to ~7 mg/kg/d, p.o.) were 13 (male 6, female 7) and 16 (male 10, female 6), respectively after 6 months treatment. Values are mean percentages (±SEM) relative to levels in young controls (8-month-old nontreated Tg2576, $n = 9$). ***C***, Levels of Tris-insoluble, formic acid-extractable $A\beta_{40}$ and $A\beta_{42}$ in cerebral cortices examined in ***B***. Values are the fold increase (±SEM) relative to levels in young controls (8-month-old nontreated Tg2576). ***D***, Aβ immunohistochemistry of coronal sections from brains of TAK-070 (bottom panel) or vehicle (top panel) treated-Tg2576 mice (13 months old). ***E***, Amyloid burden (% of area covered by Aβ immunoreactivity; left panel) or density of plaque (number per mm^2 area; right panel) in the cerebral neocortices of Tg2576 mice. Mean values (±SEM) are shown. $^{\#\#}p < 0.01$, versus those in 8-month-old mice; $^{*}p < 0.05$, $^{**}p < 0.01$, versus those in vehicle control (Student's *t* test) in ***B***, ***C***, and ***E***.

compared to those in the vehicle-treated mice (Fig. 6*D*). Quantitative analysis demonstrated that the Aβ burden (i.e., percentage area covered by Aβ immunoreactivity), as well as the number of plaques per area, were reduced by ~60% upon treatment with TAK-070 (Fig. 6*E*), in agreement with the biochemical data.

TAK-070 ameliorated behavioral deficits in Tg2576 mouse model of AD

We finally assessed the effects of TAK-070 on the behavioral deficits in Tg2576 mice. For this purpose, we conducted three different types of behavioral tests, i.e., Y-maze test, Morris water maze test and a novel object recognition test in relatively young (~5 months old) Tg2576 mice, in which behavioral impairments, along with synaptic deficits, have been documented at this stage, preceding Aβ deposition (Westerman et al., 2002; Ohno et al., 2004; Jacobsen et al., 2006).

We initially conducted Y-maze test, which has been considered as a test for spatial memory. The total arm entries of vehicle-treated Tg2576 mice ($n = 14$) were not significantly different from those of the wild-type control mice ($n = 15$). Treatment with TAK-070 for 9 d did not affect the total arm entries in Tg2576 mice (data not shown), suggesting that repeated treatment with TAK-070 did not have any effects on the basal level of exploring activity. However, the spontaneous alternation in vehicle-treated Tg2576 was significantly reduced to ~50%. This reduction was recovered by treatment with TAK-070 in a dose-dependent manner, and the ameliorating effect was significant at both dosages of 1 ($n = 14$) or 3 mg/kg ($n = 14$) (Fig. 7*A*).

We then assessed the effects of TAK-070 on impairments in spatial memory by sequentially subjecting the same cohorts to the Morris water maze test. The ability of Tg2576 mice to find an invisible platform was impaired compared to that in wild-type mice. On training day 2, significant differences in both escape latency and swimming distance remained between Tg2576 and wild-type mice, whereas they diminished on day 3. Treatment

with TAK-070 reduced the latency (Fig. 7*B*), as well as the distance (Fig. 7*C*), in a dose-dependent manner. On training day 2, the reduction in the swimming distance in TAK-070-treated Tg2576 mice (3 mg/kg) was statistically significant ($p < 0.025$, Williams' test). No significant effects were observed on the swimming speed between the vehicle- and TAK-070-treated mice (data not shown). On the next day of Morris water maze test, we obtained brains from all Tg2576 mice and measured the brain levels of Tris buffer-soluble Aβ peptides, which were decreased by ~9–16% for $A\beta_{40}$, and ~8–12% for $A\beta_{42}$, by administration of 1 and 3 mg/kg TAK-070, respectively, compared with those in vehicle-treated mice. These values were at similar levels to those observed in short-term treatment (see Fig. 6*A*).

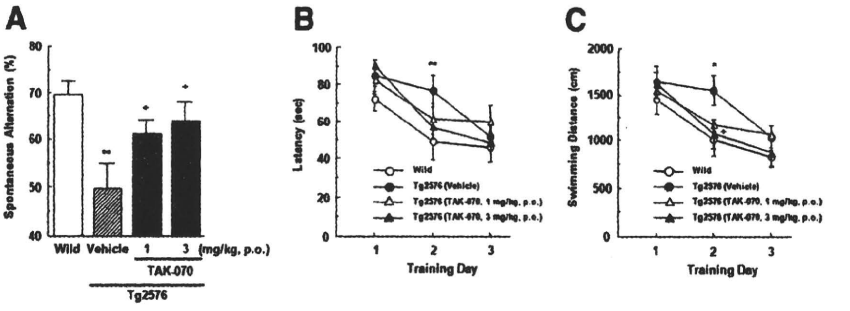

Figure 7. Effects of TAK-070 on impaired behavior of Tg2576 mice in Y-maze test and Morris water maze test. ***A***, Spontaneous alternations (as a percentage) in Y-maze test. ***B***, ***C***, Escape latency (in seconds) (***B***) and swimming distance (in centimeters) (***C***) of mice in the invisible Morris water maze test. Male Tg2576 mice (18 weeks old) were treated with TAK-070 (1 or 3 mg/kg, p.o.) or vehicle for 9 d and then sequentially tested in Y-maze on day 10 and Morris water maze tests on days 11–13. Mean values (±SEM) in 14 animals in each Tg2576 mice group and in 15 wild-type mice (Wild) are shown. $*p < 0.05$, $**p < 0.01$, versus those in Wild (Student's *t* test); $^{+}p < 0.025$, versus those in the vehicle-treated Tg2576 mice (Williams' test).

We further assessed the effects of TAK-070 on recognition memory by a novel object recognition test using new cohorts. After a 15 d successive treatment with vehicle ($n = 15$; wild type mice, $n = 14$; Tg2576) or TAK-070 (3 mg/kg, p.o., $n = 15$; Tg2576), all mice were subjected to an acquisition trial on day 1, in which mice were allowed to get access to the two identical objects in the test box. As expected, all mice equally interacted with both objects in the exploration (data not shown). On the following day, one of the two objects was replaced with a novel one and retention test was conducted. Whereas wild-type mice more frequently interacted with a novel object than a familiar object, with the novel object preference ratio of 78% (Fig. 8*A*,*B*), vehicle-treated Tg2576 mice showed a markedly decreased preference ratio of 44% (Fig. 8*B*), indicating an apparent impairment in recognition memory in Tg2576. By contrast, TAK-070 treatment significantly recovered the preference ratio to a normal range of 71% (Fig. 8*B*).

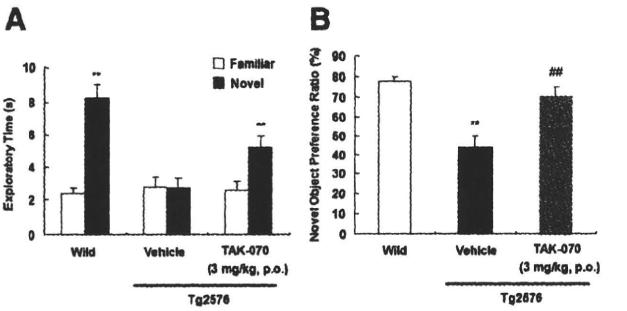

Figure 8. Effects of TAK-070 on impaired behavior of Tg2576 mice in a novel object recognition test. Mean (±SEM) time spent interacting with familiar or novel objects (***A***) and the novel object preference ratio (±SEM) (***B***) in the retention test conducted 24 h after the acquisition trial are shown. ***A***, $**p < 0.01$, versus the familiar control object. ***B***, $**p < 0.01$, versus the wild control, $^{\#\#}p < 0.01$, versus the vehicle-treated control (Student's *t* test).

Discussion

We show that TAK-070 is an orally active BACE1 inhibitor that effectively lowers the levels of soluble Aβ and increases that of sAPPα, inhibits cerebral deposition of insoluble Aβ, and rescues behavioral deficits *in vivo* in a transgenic mouse model of AD. Notably, the partial inhibition in the levels of soluble Aβ eventually resulted in a significant reduction in Aβ deposition after a 6 month chronic treatment, preserving the pharmacological efficacy at a similar level to that in a short-term treatment. We also suggest that TAK-070 exerts a unique noncompetitive inhibitory activity by interacting presumably with the transmembrane region of BACE1 outside the catalytic domain.

Multiple lines of genetic, clinical, and cell biological evidence support the causative role of Aβ in the pathogenesis of AD (for review, see Selkoe and Schenk, 2003). In contrast, sAPPα has been reported to have neurotrophic effects, e.g., promotion of synapse formation or amelioration of cognitive deficits [for review, see Isacson et al. (2002) and Postina (2008)]. In our present study, untreated, aged Tg2576 mice had lower brain levels of sAPPα and higher soluble Aβ with aging, in agreement with previous observations that BACE1 activity is upregulated with aging in the brains of animals as well as humans (Fukumoto et al., 2004; Zohar et al., 2005). Hence, manipulation of APP processing by BACE1 inhibition in a way to reduce Aβ and increase sAPPα would be a rational strategy for the treatment and prevention of AD.

The chemical structure of TAK-070 differs markedly from that of peptide-based BACE1 inhibitors (for review, see Silvestri, 2009). However our cellular and cell-free assay data clearly indicated that TAK-070 is a bona fide BACE1 inhibitor. Cell-free study showed that TAK-070 directly and specifically inhibited full-length BACE1 without affecting other aspartic proteases. TAK-070 reduced levels of secreted Aβ and sAPPβ, together with an increase in sAPPα in cultured cells (Fig. 3), which are in agreement with the previous results of antisense oligonucleotide study for BACE1 (Vassar et al., 1999). The Lineweaver–Burk plot analysis revealed that TAK-070 is a noncompetitive inhibitor (Fig. 4), which was supported by the surface plasmon resonance assay. TAK-070 did bind to the full-length BACE1 (1-501) and truncated BACE1 (1-471 and 474), but not to the truncated BACE1 (1-454, 460, and 465) (Fig. 5). This suggests that TAK-070 inhibits BACE1 activity in a unique mode of interaction by binding to the ~10 aa residues in the C-terminal region (residues 465–474) within the transmembrane domain, but not to the catalytic center (located in residues 93–96 and 289–293). Surface plasmon resonance assay also showed that TAK-070 does not interact with APP(18-688) or sAPPβ (supplemental Fig. S3, available at www.jneurosci.org as supplemental material). This suggests that TAK-070 does not affect APP processing by binding to subdomain of APP containing the BACE1-cleavage sites. We were not able to completely rule out the possibility that TAK-070 interacts with the transmembrane domain of APP, like benzofuran-containing compounds that bind C99 (Espeseth et al., 2005). However, TAK-070 failed to inhibit Aβ secretion from HEK293 cells overexpressing C99 (data not shown), supporting the notion

that TAK-070 does not target C99 in APP. In addition, the possibility that TAK-070 is an α-secretase activator was excluded by (1) the lack of increase in the protein levels of α-secretase candidate, i.e., ADAM10 (Fig. 3), (2) lack of inhibition of TACE activity using a peptidic substrate in a cell-free assay (data not shown), and (3) the lack of increase in α-secretase activity in a cell-based assay (supplemental Fig. S2, available at www.jneurosci.org as supplemental material).

The potency of TAK-070 to reduce the Aβ secretion in cell cultures was modest (i.e., ~25% reduction was achieved at 3 μmol/L with a MEC of ~0.1–0.3 μmol/L in N2aAPPsw cells) (Fig. 2). These results were in agreement with the relatively modest BACE1-inhibitory effect in the cell-free assay with IC_{35} of ~3.15 μmol/L and MEC at ~0.1 μmol/L (Fig. 4). Interestingly, however, we observed similar levels of reduction in soluble Aβ by ~20% in the brains of Tg2576 mice (Fig. 6*A*,*B*). Although small chemicals generally have less potency in brains, hampered by the blood–brain-barrier and cell-penetration issues, this relatively high potency of TAK-070 is likely to be attributable to the highly lipophilic structure bearing *N*-alkyl-amine moiety. In fact, a single administration of TAK-070 in rat (3 mg/kg, p.o.) yielded effective concentration of ~2 μmol/L in brain with the T_{max} of ~24 h using ^{14}C-TAK-070, and the brain exposure levels in short-term- and long-term-treated Tg2576 mice were ~8 μmol/L and ~6–11 μmol/L, respectively (56 ppm of TAK-070, corresponding to ~7–8 mg/kg) (Fig. 6) (our unpublished observations). Furthermore, it has been reported that full-length BACE1, forming a high-molecular-weight complex associated with lipid, exhibits higher enzymatic activity than that of C-terminally truncated BACE1 (1-454) (Marlow et al., 2003; Westmeyer et al., 2004). This may support the view that lipophilic TAK-070 effectively reaches the membrane-associated BACE1 complex.

TAK-070 exhibits ceiling effects on reduction in Aβ and increase in sAPPα (Figs. 2, 6*A*), which may partly be explained by the noncompetitive inhibitory profile for BACE1. We have also observed similar plateau effects in normal rats with a minimum effective dose of 0.1 mg/kg after 4 week administration (our unpublished observation). However, long-term treatment with TAK-070 led to more pronounced Aβ-lowering effects on insoluble Aβ (Fig. 6*C–E*) than on soluble Aβ (Fig. 6*A*,*B*). This finding dovetails with the observation in BACE1 heterozygous KO crossed with PDAPP transgenic mice, in which soluble Aβ levels were lowered only by 12% at a young age, whereas Aβ-accumulation was eventually reduced by ~50–90% with synaptic amelioration in elderly animals (McConlogue et al., 2007). Together, these results strongly suggest that partial inhibition of BACE1, causing partial reduction in Aβ and increase in sAPPα, has sufficient pharmacological efficacy on normalization of APP processing and cognitive functions.

Behavioral deficits in Tg2576 mice have been reported to occur before the deposition of Aβ plaques (Westerman et al., 2002; Ohno et al., 2004; Jacobsen et al., 2006), which may be due to the accumulation of toxic forms of Aβ, e.g., oligomers, that leads to the deterioration of synaptic functions and behaviors (Walsh et al., 2002; Cleary et al., 2005; Venkitaramani et al., 2007). In the present study, relatively young (~5 months) Tg2576 mice showed impairment in behaviors both in Y-maze and novel object recognition tests, whereas the deficits in Morris water maze test were modest, with no differences in the acquisition trial on day 3 between Tg2576 and wild-type cohorts. TAK-070 ameliorated all these behavioral deficits by a short-term treatment at biochemically effective doses (1–3 mg/kg, p.o.) (Figs. 7, 8). TAK-070 had ameliorative effects in the Y-maze and Morris water maze tests that reflect the hippocampal-dependent learning, in line with observations in BACE1 homozygous KO/APP transgenic bigenic mice (Ohno et al., 2004, 2006, 2007). However, there were pivotal differences: TAK-070 treatment affected neither the total number of arm entry in Y-maze test (Ohno et al., 2004) nor the swimming speed in Morris water maze test (Ohno et al., 2006), which were documented to be abnormal in BACE1-homozygous KO regardless of APP-transgenic background. Furthermore, BACE1-homozygous KO in nontransgenic background have been reported to show cognitively deteriorative (Ohno et al., 2004, 2006, 2007), schizophrenia-like (Savonenko et al., 2008), or hypomyelination (Hu et al., 2006; Sankaranarayanan et al., 2008) phenotypes, underscoring the necessity of BACE1 activity for physiological functions, probably due to multiplicity of substrates for BACE1 (for review, see Marks and Berg, 2008). Also in nontransgenic aged rats, TAK-070 ameliorated behavioral deficits in the water maze test (our unpublished observation). Hence, TAK-070 appears to be pharmacologically effective and safe by partial BACE1 inhibition, avoiding adverse events due to complete inhibition of BACE1.

It is noteworthy that the pharmacological effects of orally administered TAK-070 for ~6 months on the brain levels of soluble Aβ and sAPPα were similar to those in short-term treatment (Fig. 6*A*,*B*). Under the chronic treatment, mice were tolerable to TAK-070 and survived comparable to vehicle control after ~6 months. These profiles should be a merit of this compound, considering the long period of AD medication. The sustained efficacy of TAK-070 markedly differs from those documented in other BACE1 inhibitors (Sankaranarayanan et al., 2008) or on the higher efficacy of a compound in the presence of inhibitors of P-glycoprotein (Hussain et al., 2007), that determines exposure levels of compounds in brains.

In sum, the successful treatment by a noncompetitive BACE1 inhibitor, TAK-070, provides strong support for the validity of partial BACE1 inhibition as a disease-modifying as well as symptomatic therapy for AD. TAK-070 will also provide a clue for the elucidation of the mechanism of noncompetitive regulation of the activity of BACE1.

References

Asami-Odaka A, Ishibashi Y, Kikuchi T, Kitada C, Suzuki N (1995) Long amyloid β-protein secreted from wild-type human neuroblastoma IMR-32 cells. Biochemistry 34:10272–10278.

Chen Q, Nakajima A, Choi SH, Xiong X, Tang YP (2008) Loss of presenilin function causes Alzheimer's disease-like neurodegeneration in the mouse. J Neurosci Res 86:1615–1625.

Cleary JP, Walsh DM, Hofmeister JJ, Shankar GM, Kuskowski MA, Selkoe DJ, Ashe KH (2005) Natural oligomers of the amyloid-β protein specifically disrupt cognitive function. Nat Neurosci 8:79–84.

Cole SL, Vassar R (2008) BACE1 structure and function in health and Alzheimer's disease. Curr Alzheimer Res 5:100–120.

Doedens JR, Mahimkar RM, Black RA (2003) TACE/ADAM-17 enzymatic activity is increased in response to cellular stimulation. Biochem Biophys Res Commun 308:331–338.

Donoviel DB, Hadjantonakis AK, Ikeda M, Zheng H, Hyslop PS, Bernstein A (1999) Mice lacking both presenilin genes exhibit early embryonic patterning defects. Genes Dev 13:2801–2810.

Espeseth AS, Xu M, Huang Q, Coburn CA, Jones KLG, Ferrer M, Zuck PD, Strulovici B, Price EA, Wu G, Wolfe AL, Lineberger JE, Sardana M, Tugusheva K, Pietrak BL, Crouthamel M-C, Lai M-T, Dodson EC, Bazzo R, Shi X-P, et al. (2005) Compounds that bind APP and inhibit Aβ processing in vitro suggest a novel approach to Alzheimer disease therapeutics. J Biol Chem 280:17792–17797.

Fukumoto H, Tomita T, Matsunaga H, Ishibashi Y, Saido TC, Iwatsubo T (1999) Primary cultures of neuronal and non-neuronal rat brain cells secrete similar proportions of amyloid β peptides ending at Aβ40 and Aβ42. Neuroreport 10:2965–2969.

Fukumoto H, Rosene DL, Moss MB, Raju S, Hyman BT, Irizarry MC (2004) β-secretase activity increases with aging in human, monkey, and mouse brain. Am J Pathol 164:719–725.

Hu X, Hicks CW, He W, Wong P, Macklin WB, Trapp BD, Yan R (2006) Bace1 modulates myelination in the central and peripheral nervous system. Nat Neurosci 9:1520–1525.

Hussain I, Hawkins J, Harrison D, Hille C, Wayne G, Cutler L, Buck T, Walter D, Demont E, Howes C, Naylor A, Jeffrey P, Gonzalez MI, Dingwall C, Michel A, Redshaw S, Davis JB (2007) Oral administration of a potent and selective non-peptidic BACE-1 inhibitor decreases β-cleavage of amyloid precursor protein and amyloid-β production in vivo. J Neurochem 100:802–809.

Isacson O, Seo H, Lin L, Albeck D, Granholm AC (2002) Alzheimer's disease and Down's syndrome: roles of APP, trophic factors and ACh. Trends Neurosci 25:79–84.

Iwatsubo T, Odaka A, Suzuki N, Mizusawa H, Nukina N, Ihara Y (1994) Visualization of Aβ42(43) and Aβ40 in senile plaques with end-specific Aβ monoclonals: evidence that an initially deposited species is Aβ42(43). Neuron 13:45–53.

Jacobsen JS, Wu CC, Redwine JM, Comery TA, Arias R, Bowlby M, Martone R, Morrison JH, Pangalos MN, Reinhart PH, Bloom FE (2006) Early-onset behavioral and synaptic deficits in a mouse model of Alzheimer's disease. Proc Natl Acad Sci U S A 103:5161–5166.

Jorissen E, Prox J, Bernreuther C, Weber S, Schwanbeck R, Serneels L, Snellinx A, Craessaerts K, Thathiah A, Tesseur I, Bartsch U, Weskamp G, Blobel CP, Glatzel M, De Strooper B, Saftig P (2010) The disintegrin/metalloproteinase ADAM10 is essential for the establishment of the brain cortex. J Neurosci 30:4833–4844.

Lakshmana MK, Yoon IS, Chen E, Bianchi E, Koo EH, Kang DE (2009) Novel role of RanBP9 in BACE1 processing of amyloid precursor protein and amyloid β peptide generation. J Biol Chem 284:11863–11872.

Marks N, Berg MJ (2008) Neurosecretases provide strategies to treat sporadic and familial Alzheimer disorders. Neurochem Int 52:184–215.

Marlow L, Cain M, Pappolla MA, Sambamurti K (2003) β-Secretase processing of the Alzheimer's amyloid protein precursor (APP). J Mol Neurosci 20:233–239.

McConlogue L, Buttini M, Anderson JP, Brigham EF, Chen KS, Freedman SB, Games D, Johnson-Wood K, Lee M, Zeller M, Liu W, Motter R, Sinha S (2007) Partial reduction of BACE1 has dramatic effects on Alzheimer plaque and synaptic pathology in APP transgenic mice. J Biol Chem 282:26326–26334.

Obregon DF, Rezai-Zadeh K, Bai Y, Sun N, Hou H, Ehrhart J, Zeng J, Mori T, Arendash GW, Shytle D, Town T, Tan J (2006) ADAM10 activation is required for green tea (-)-epigallocatechin-3-gallate-induced (alpha)-secretase cleavage of amyloid precursor protein. J Biol Chem 281:16419–16427.

Ohno M, Sametsky EA, Younkin LH, Oakley H, Younkin SG, Citron M, Vassar R, Disterhoft JF (2004) BACE1 deficiency rescues memory deficits and cholinergic dysfunction in a mouse model of Alzheimer's disease. Neuron 41:27–33.

Ohno M, Chang L, Tseng W, Oakley H, Citron M, Klein WL, Vassar R, Disterhoft JF (2006) Temporal memory deficits in Alzheimer's mouse models: rescue by genetic deletion of BACE1. Eur J Neurosci 23:251–260.

Ohno M, Cole SL, Yasvoina M, Zhao J, Citron M, Berry R, Disterhoft JF, Vassar R (2007) BACE1 gene deletion prevents neuron loss and memory deficits in 5XFAD APP/PS1 transgenic mice. Neurobiol Dis 26:134–145.

Postina R (2008) A closer look at α-secretase. Curr Alzheimer Res 5:179–186.

Sankaranarayanan S, Price EA, Wu G, Crouthamel MC, Shi XP, Tugusheva K, Tyler KX, Kahana J, Ellis J, Jin L, Steele T, Stachel S, Coburn C, Simon AJ (2008) In vivo beta-secretase 1 inhibition leads to brain Aβ lowering and increased α-secretase processing of amyloid precursor protein without effect on neuregulin-1. J Pharmacol Exp Ther 324:957–969.

Sankaranarayanan S, Holahan MA, Colussi D, Crouthamel MC, Devanarayan V, Ellis J, Espeseth A, Gates AT, Graham SL, Gregro AR, Hazuda D, Hochman JH, Holloway K, Jin L, Kahana J, Lai MT, Lineberger J, McGaughey G, Moore KP, Nantermet P, et al. (2009) First demonstration of cerebrospinal fluid and plasma Aβ lowering with oral administration of a β-site amyloid precursor protein-cleaving enzyme 1 inhibitor in nonhuman primates. J Pharmacol Exp Ther 328:131–140.

Saura CA, Choi SY, Beglopoulos V, Malkani S, Zhang D, Shankaranarayana Rao BS, Chattarji S, Kelleher RJ 3rd, Kandel ER, Duff K, Kirkwood A, Shen J (2004) Loss of presenilin function causes impairments of memory and synaptic plasticity followed by age-dependent neurodegeneration. Neuron 42:23–36.

Saura CA, Chen G, Malkani S, Choi SY, Takahashi RH, Zhang D, Gouras GK, Kirkwood A, Morris RG, Shen J (2005) Conditional inactivation of presenilin 1 prevents amyloid accumulation and temporarily rescues contextual and spatial working memory impairments in amyloid precursor protein transgenic mice. J Neurosci 25:6755–6764.

Savonenko AV, Melnikova T, Laird FM, Stewart KA, Price DL, Wong PC (2008) Alteration of BACE1-dependent NRG1/ErbB4 signaling and schizophrenia-like phenotypes in BACE1-null mice. Proc Natl Acad Sci U S A 105:5585–5590.

Selkoe DJ, Schenk D (2003) Alzheimer's disease: molecular understanding predicts amyloid-based therapeutics. Annu Rev Pharmacol Toxicol 43:545–584.

Shen J, Bronson RT, Chen DF, Xia W, Selkoe DJ, Tonegawa S (1997) Skeletal and CNS defects in Presenilin-1-deficient mice. Cell 89:629–639.

Silvestri R (2009) Boom in the development of non-peptidic β-secretase (BACE1) inhibitors for the treatment of Alzheimer's disease. Med Res Rev 29:295–338.

Sinha S, Anderson JP, Barbour R, Basi GS, Caccavello R, Davis D, Doan M, Dovey HF, Frigon N, Hong J, Jacobson-Croak K, Jewett N, Keim P, Knops J, Lieberburg I, Power M, Tan H, Tatsuno G, Tung J, Schenk D, et al. (1999) Purification and cloning of amyloid precursor protein β-secretase from human brain. Nature 402:537–540.

Stockley JH, O'Neill C (2007) The proteins BACE1 and BACE2 and β-secretase activity in normal and Alzheimer's disease brain. Biochem Soc Trans 35:574–576.

Takahashi Y, Hayashi I, Tominari Y, Rikimaru K, Morohashi Y, Kan T, Natsugari H, Fukuyama T, Tomita T, Iwatsubo T (2003) Sulindac sulfide is a noncompetitive γ-secretase inhibitor that preferentially reduces Aβ42 generation. J Biol Chem 278:18664–18670.

Tomita T, Katayama R, Takikawa R, Iwatsubo T (2002) Complex N-glycosylated form of nicastrin is stabilized and selectively bound to presenilin fragments. FEBS Lett 520:117–121.

Vassar R, Bennett BD, Babu-Khan S, Kahn S, Mendiaz EA, Denis P, Teplow DB, Ross S, Amarante P, Loeloff R, Luo Y, Fisher S, Fuller J, Edenson S, Lile J, Jarosinski MA, Biere AL, Curran E, Burgess T, Louis JC, et al. (1999) β-secretase cleavage of Alzheimer's amyloid precursor protein by the transmembrane aspartic protease BACE. Science 286:735–741.

Venkitaramani DV, Chin J, Netzer WJ, Gouras GK, Lesne S, Malinow R, Lombroso PJ (2007) β-Amyloid modulation of synaptic transmission and plasticity. J Neurosci 27:11832–11837.

Walsh DM, Klyubin I, Fadeeva JV, Cullen WK, Anwyl R, Wolfe MS, Rowan MJ, Selkoe DJ (2002) Naturally secreted oligomers of amyloid beta protein potently inhibit hippocampal long-term potentiation in vivo. Nature 416:535–539.

Westerman MA, Cooper-Blacketer D, Mariash A, Kotilinek L, Kawarabayashi T, Younkin LH, Carlson GA, Younkin SG, Ashe KH (2002) The relationship between Aβ and memory in the Tg2576 mouse model of Alzheimer's disease. J Neurosci 22:1858–1867.

Westmeyer GG, Willem M, Lichtenthaler SF, Lurman G, Multhaup G, Assfalg-Machleidt I, Reiss K, Saftig P, Haass C (2004) Dimerization of β-site β-amyloid precursor protein-cleaving enzyme. J Biol Chem 279:53205–53212.

Wong PC, Zheng H, Chen H, Becher MW, Sirinathsinghji DJ, Trumbauer ME, Chen HY, Price DL, Van der Ploeg LH, Sisodia SS (1997) Presenilin 1 is required for Notch1 and DII1 expression in the paraxial mesoderm. Nature 387:288–292.

Zohar O, Pick CG, Cavallaro S, Chapman J, Katzav A, Milman A, Alkon DL (2005) Age-dependent differential expression of BACE splice variants in brain regions of tg2576 mice. Neurobiol Aging 26:1167–1175.

Neurobiology of Disease

Participation of Transmembrane Domain 1 of Presenilin 1 in the Catalytic Pore Structure of the γ-Secretase

Shizuka Takagi (高木穏香),[1] Aya Tominaga (富永綾),[1] Chihiro Sato (佐藤千尋),[1,2,3] Taisuke Tomita (富田泰輔),[1,2] and Takeshi Iwatsubo (岩坪威)[1,2,3]

[1]Department of Neuropathology and Neuroscience, Graduate School of Pharmaceutical Sciences, The University of Tokyo, Tokyo 113-0033, Japan, [2]Core Research for Evolutional Science and Technology, Japan Science and Technology Corporation, and [3]Department of Neuropathology, Graduate School of Medicine, The University of Tokyo, Hongo 7-3-1, Bunkyo, Tokyo 113-0033, Japan

γ-Secretase is an intramembrane-cleaving protease that is responsible for the generation of amyloid-β peptides linked to the pathogenesis of Alzheimer's disease. Using a substituted cysteine accessibility method, we have previously shown that the hydrophilic "catalytic pore" structure of γ-secretase is formed by the transmembrane domains (TMDs) 6, 7, and 9 of presenilin 1 (PS1), the catalytic subunit of γ-secretase, within the membrane. Here, we analyzed the structure in and around the first hydrophobic region, the putative TMD1, of PS1, of which the precise function as well as three-dimensional location within γ-secretase remained unknown. We found that TMD1 is located in proximity to the catalytic GxGD and PAL motifs within the C-terminal fragment of PS1, facing directly the catalytic pore. Competition experiments using known γ-secretase inhibitors suggested that the N-terminal region of TMD1 functions as a subsite during proteolytic action of the γ-secretase. Intriguingly, binding of inhibitors affected water accessibility of residues at the membrane border of TMD1, suggesting the possibility of a dynamic motion of TMD1 during the catalytic process. Our results provide mechanistic insights into the functional role of TMD1 of PS1 in the intramembrane-cleaving activity of the γ-secretase.

Introduction

The process of generation and deposition of amyloid-β peptide (Aβ) is strongly implicated in the pathogenesis of Alzheimer/s disease (AD) (Haass and Selkoe, 2007). Accordingly, γ-secretase, a protease responsible for the Aβ generation, is one of the plausible therapeutic targets for AD (Tomita, 2009; De Strooper et al., 2010). However, γ-secretase cleaves several type I single-span membrane proteins, including Notch receptor. Thus, the mechanism-based rational design of γ-secretase inhibitors (GSIs) based on the structural information of the γ-secretase is unequivocally needed for development of AD therapeutics. γ-Secretase is an unconventional aspartyl protease that hydrolyzes its substrates within the hydrophobic lipid bilayer. It belongs to a unique group of intramembrane-cleaving proteases (I-CLiPs), of which site 2 protease (S2P), signal peptide peptidase, and rhomboid have been identified as other members (Wolfe and Kopan, 2004). The recently resolved crystal structures of the rhomboid and S2P have shed light on the possible mechanism as to how peptide bond hydrolysis can take place within the lipid environment (Urban and Shi, 2008). Nonetheless, structural analysis such as x-ray crystallography is still an extremely challenging task for multimeric membrane protein complexes (e.g., the γ-secretase), which is comprised of nicastrin, anterior pharynx defective-1, presenilin enhancer-2, and PS (Takasugi et al., 2003). We have been applying substituted cysteine accessibility method (SCAM) to gain insights into the structure of presenilin 1 (PS1) in a membrane-embedded state. SCAM has been reiteratively used to obtain structural information of various multipass membrane proteins in a functional state, by covalently modifying the introduced cysteine (Cys) residues using sulfhydryl reagents (Karlin and Akabas, 1998; Kaback et al., 2001). Using SCAM, we and others have revealed that PS1 harbors a hydrophilic "catalytic pore" formed by transmembrane domains (TMDs) 6, 7, and 9 (Sato et al., 2006, 2008; Tolia et al., 2006, 2008). Recent nuclear magnetic resonance analysis of the C-terminal region of PS1 supported the results of SCAM analysis (Sobhanifar et al., 2010). This was consistent with the structures obtained from the crystallographic analyses of rhomboid and S2P, further suggesting that the hydrophilic milieu around the active site located within the lipid bilayer is a common structure across I-CLiPs. Meanwhile, recent chemical biological studies revealed that several GSIs directly target the N-terminal fragment (NTF) of PS1 (Fuwa et al., 2007; Imamura et al., 2009). Thus, an important remaining question regarding the structure–function relationship of γ-secretase is how the other five TMDs within the PS1 NTF contribute to the γ-secretase activity. Here, we used

Received June 26, 2010; revised Sept. 12, 2010; accepted Sept. 23, 2010.

This work was supported by Grants-in-Aid for Young Scientists (S) (to T.T.) from the Ministry of Education, Culture, Sports, Science, and Technology of Japan (MEXT), by Scientific Research on Priority Areas "Research on Pathomechanisms of Brain Disorders" from MEXT (to T.T., T.I.), by the Program for Promotion of Fundamental Studies in Health Sciences of the National Institute of Biomedical Innovation (to T.T., T.I.), by Targeted Proteins Research Program of the Japan Science and Technology Corporation (JST) (to T.T., T.I.), and by Core Research for Evolutional Science and Technology of JST (to T.T., T.I.), Japan. S.T. and C.S. are research fellows of the Japan Society for the Promotion of Science. We thank Drs. G. Thinakaran (University of Chicago, Chicago, IL) for antibodies, B. De Strooper (KU Leuven, Leuven, Belgium) for DKO cells, T. Kitamura (University of Tokyo, Tokyo, Japan) for retroviral infection system, and Takeda Pharmaceutical Company for Aβ ELISA. We are also grateful to our laboratory members for helpful discussions and technical assistance.

Correspondence should be addressed to Dr. Taisuke Tomita, Department of Neuropathology and Neuroscience, Graduate School of Pharmaceutical Sciences, The University of Tokyo, 7-3-1 Hongo, Bunkyo-ku, Tokyo 113-0033, Japan. E-mail: taisuke@mol.f.u-tokyo.ac.jp.

DOI:10.1523/JNEUROSCI.3318-10.2010

 0270-6474/10/3015943-08$15.00/0

SCAM and other biochemical methods to analyze the structure and the functional role of TMD1 of PS1, which has been shown to be indispensable for the stability, as well as the catalytic activity, of the γ-secretase (Watanabe et al., 2005, 2010).

Materials and Methods

G1L3, which recognizes the hydrophilic loop 6 of PS1, was described previously (Tomita et al., 1999). Anti-$PS1_{NT}$ (Thinakaran et al., 1998) was kindly provided by Dr. Thinakaran (University of Chicago, Chicago, IL). Other antibodies were purchased from BD Biosciences (anti-E-cadherin), Cell Signaling Technology [anti-cleaved Notch1 (V1744) and anti-myc tag (9B11)], or Sigma [anti-α-tubulin (DM1A)]. {1*S*-Benzyl-4*R*-[1-(1*S*-carbamoyl-2-phenylethylcarbamoyl)-1*S*-3-methyl-butylcarbamoyl]-2*R*-hydroxy-5-phenylpentyl}carbamic acid *tert*-butyl ester (L-685,458) (Shearman et al., 2000) and peptide 15 (pep15) (Das et al., 2003) were purchased from Bachem and BEX, respectively. *N*-[*N*-(3,5-difluorophenacetyl)]-*L*-alanyl]-*S*-phenylglycine *tert*-butyl ester (DAPT) was synthesized as described previously (Dovey et al., 2001; Kan et al., 2004). All 3-(4,5-dimethylthiazol-2-yl)-5-(3-carboxymethoxyphenyl)-2-(4-sulfophenyl)-2*H*-tetrazolium (MTS) reagents (Toronto Research Chemicals) were dissolved in DMSO at 200 mM and stored at −80°C until use. The abbreviations used for MTS cross-linkers are described previously (Sato et al., 2006, 2008). cDNAs encoding APP_{NL}, NotchΔE, PS1, and Cysless PS1 [PS1/Cys(−)] were described previously (Kopan et al., 1996; Tomita et al., 1997; Sato et al., 2006). Single- or double-Cys mutant (mt) PS1 cDNAs were generated using a long PCR-based protocol. Maintenance of embryonic fibroblasts derived from *Psen1/Psen2* double knock-out (DKO) cells (Herreman et al., 2000), a retroviral infection system (Kitamura et al., 2003), and generation of stable infectants was performed as described previously (Watanabe et al., 2005, 2010; Sato et al., 2006, 2008). Microsome preparation and immunoblot analysis were performed as described previously (Tomita et al., 1997, 1999, 2001; Takahashi et al., 2003; Hayashi et al., 2004). For the measurement of secreted Aβ, recombinant retrovirus encoding each Cys mt PS1 was transiently infected into DKO cells that stably expressing APP_{NL} (Watanabe et al., 2005). After 24 h incubation, the conditioned medium was collected and subjected to two-site ELISAs (i.e., BAN50/BA27 and BAN50/BC05 for Aβ40 and Aβ42, respectively) (Iwatsubo et al., 1994, Tomita et al., 1997, 1998, 2001). Biotinylation and competition experiments using *N*-biotinylaminoethyl methanethiosulfonate (MTSEA-biotin) in intact cells or microsome fraction have been described in detail before (Sato et al., 2006, 2008; Isoo et al., 2007). Cross-linking experiments were performed as previously described except that the microsomes were prepared from 10 cm dishes per single analysis. For a competition assay, sodium 2-sulfonatoethyl methanethiosulfonate (MTSES), 2-(trimethylammonium)ethyl methanethiosulfonate bromide (MSTET), or 2-(triethylammonium)ethyl methanethiosulfonate (MTS-TEAE) was preincubated with intact cells or microsomes at 2 mM for 5 min at 4°C and washed once before biotinylation. GSIs were preincubated with microsome aliquots for 30 min at room temperature before incubation with cross-linkers. The inhibitors were used at concentrations (L-685,458, 1 μM; DAPT, 10 μM; pep15, 1 μM) that completely abolish the proteolytic activity of γ-secretase (Morohashi et al., 2006; Sato et al., 2006).

Results

SCAM analysis of the hydrophobic region 1 of PS1

Previous computational predictions and cell-based topological studies indicated that the hydrophobic region (HR) 1 of PS1 spans the membrane as TMD1 (Doan et al., 1996; Li and Greenwald, 1996; Lehmann et al., 1997; Nakai et al., 1999). To examine whether this region penetrates the membrane as a TMD and faces to the aqueous environment in the lipid bilayer, we constructed mutant PS1 having a single cysteine residue based on PS1/Cys(−) (single-Cys mt PS1) at 32 different amino acid residues in and around the HR1 (E71-V103), and expressed them in DKO cells (Fig. 1). We excluded V96C from further analyses, because Cys substitution of V96 resulted in loss of expression of PS1 polypeptide and failure in the restoration of the γ-secretase activity (supplemental Fig. 1, available at www.jneurosci.org as supplemental material). All the other single-Cys mt PS1 retained the protein expression, endoproteolysis, and the γ-secretase activity. SCAM analysis of the single-Cys mt PS1 in intact cells revealed that V94C, I100C, K101C, S102C, and V103C were biotinylated by MTSEA-biotin (Fig. 2, top), suggesting that these labeled residues are located in a hydrophilic milieu accessible from the extracel-

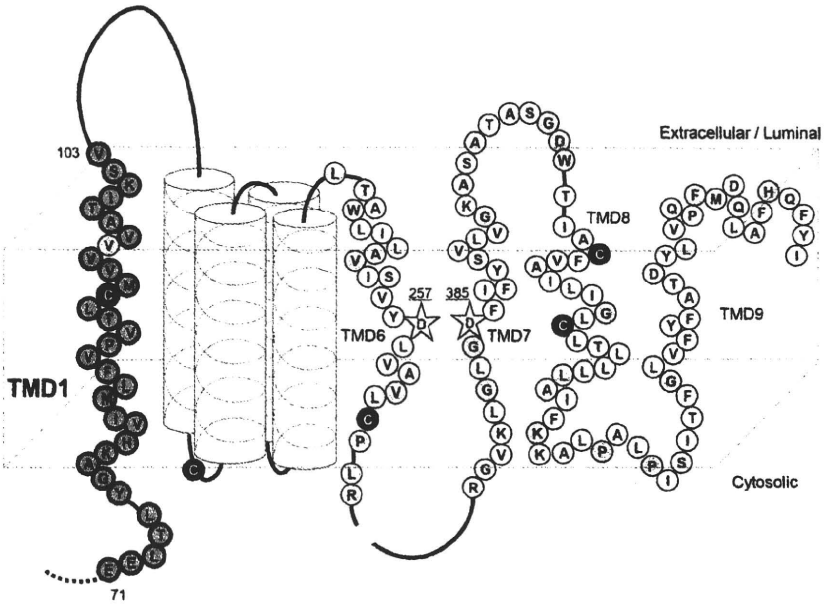

Figure 1. Locations of the PS1 cysteine mutations used in this study. Schematic depiction of human PS1 is shown. Endogenous Cys residues that were replaced with serine in PS1/Cys(−) are indicated as black circles. Amino acid residues substituted to Cys in the present and previous studies are shown by circles with a single-letter character representing the original amino acids. Residues analyzed in this study are indicated by orange circles. Residues in which Cys substitution caused a loss of γ-secretase activity are indicated as gray circles. Catalytic aspartates are shown by yellow stars.

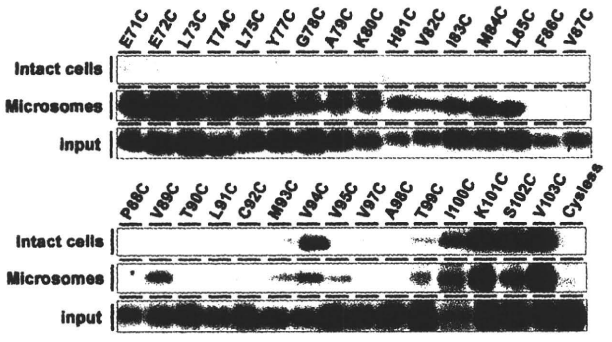

Figure 2. SCAM analysis of single-Cys mt PS1 around HR1. Intact cells (top) expressing single-Cys mt PS1 or the microsomes (middle) were incubated with MTSEA-biotin. Biotinylated proteins were precipitated with streptavidin beads and then subjected to immunoblot analysis. Cysless serves as the negative control. Amount of PS1 NTF in the input fraction is shown in the bottom panel.

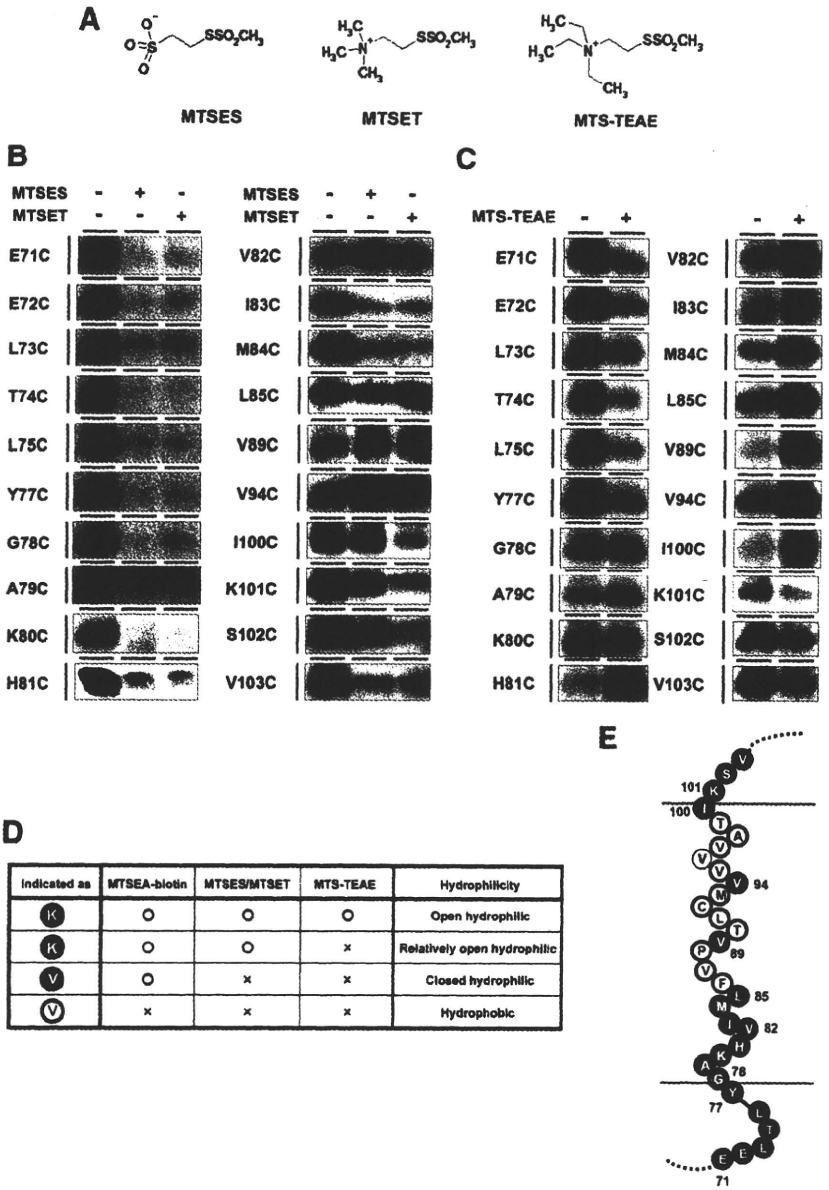

Indicated as	MTSEA-biotin	MTSES/MTSET	MTS-TEAE	Hydrophilicity
K	○	○	○	Open hydrophilic
K	○	○	×	Relatively open hydrophilic
V	○	×	×	Closed hydrophilic
V	×	×	×	Hydrophobic

Figure 3. SCAM analysis of single-Cys mt PS1 using charged MTS reagents. ***A***, The structures of the charged MTS reagents. The abbreviations are indicated below in ***B***. ***B***, Labeling competition of single-Cys mt PS1 around HR1 was examined after preincubation with negatively charged MTSES or positively charged MTSET. ***C***, Labeling competition experiments using positively charged MTS-TEAE with a bulkier structure. ***D***, Summary of the competition experiments using charged MTS reagents. ***E***, Schematic depiction of TMD1. All charged reagents were accessible to the Cys-substituted residues indicated by blue circles. Residues whose labeling was competed by MTSES or MTSET, but not by MTS-TEAE, are indicated by sky-blue circles. Residues whose labeling was not decreased by any charged reagents are indicated by purple circles. Residues that were not labeled by MTSEA-biotin or unanalyzed are shown by black letters in white and gray circles, respectively. The predicted lipid–water interface is indicated by green lines.

lular side. We next examined the accessibility of MTSEA-biotin to these residues from either the extracellular/luminal or cytosolic sides using microsome fractions from DKO cells expressing single-Cys mt PS1, which have been shown to be composed of a mixture of inside-out and outside-out vesicles (Sato et al., 2006). In addition to the residues that were biotinylated in intact cells, consecutive amino acid residues from E71C to L85C, as well as V89C, were positively labeled with MTSEA-biotin (Fig. 2, middle). The densitometric quantitation of each band is shown in supplemental Figure 2 (available at www.jneurosci.org as supplemental material). These results are consistent with the view that HR1 region spans the lipid bilayer with a type II orientation. Next, we analyzed the steric and electrostatic environment around the water-accessible residues using other membrane-impermeable MTS derivatives (i.e., the negatively charged MTSES and positively charged MTSET) as competitors for MTSEA-biotin (Fig. 3*A*, left and middle) (Sato et al., 2006, 2008). Preincubation with MTSES or MTSET failed to decrease the labeling of V82C, L85C, V89C, and V94C by MTSEA-biotin, whereas the biotinylation of other mutants was abolished by both of the charged MTS reagents (Fig. 3*B*). These data suggest that V82, L85, V89, and V94 are located in a closed hydrophilic environment with limited access to outside within the lipid bilayer. In contrast, other residues in which MTSES and MTSET competed for biotinylation were predicted to be facing an open hydrophilic environment. To further analyze the open hydrophilic environment in detail, we used MTS-TEAE, a sterically bulkier derivative of MTSET (Fig. 3*A*, right). As expected, preincubation with MTS-TEAE did not compete for the biotinylation of the Cys residues to which MTSES or MTSET was inaccessible (i.e., V82C, L85C, V89C, or V94C). However, MTS-TEAE failed to decrease the labeling of G78C, A79C, K80C, H81C, I83C, M84C, and I100C, although the biotinylation of these mutants was competed for that by MTSES or MTSET, suggesting that these residues are located within a relatively open, but sterically hindered, hydrophilic environment. In contrast, the labeling of other mutants (i.e., from E71C through Y77C and K101 through V103C) was decreased by preincubation with MTS-TEAE (Fig. 3*C*). These data indicate that the residues from E71 to Y77 and K101 to V103 are exposed to an open hydrophilic environment with unlimited access at the cytosolic and extracellular sides, respectively (for a summary, see Fig. 3*D*,*E*). Strong labeling of these residues by MTSEA-biotin also supports this notion (Fig. 2; supplemental Fig. 2, available at www.jneurosci.org as supplemental material). Intriguingly, the

Table 1. The summary of the cross-linking experiments in this study

	MTS cross-linkers		
	M84C	V89C	V94C
L383C at GxGD motif	M2M (<5.2 Å)	M2M (<5.2 Å)	M8M (<13.0 Å)
I387C	M8M (<13.0 Å)	M8M (<13.0 Å)	Not cross-linked
L435C at PAL motif	M11M (<16.9 Å)	M2M (<5.2 Å)	ND

"MTS cross-linkers" indicates the abbreviated name of the shortest cross-linker that enabled the production of an NTF-CTF heterodimer (i.e., M2M). Values in parentheses indicate the length of the spacer arm of the MTS cross-linkers. ND, Not determined.

biotinylation of some residues was dramatically augmented by preincubation with the membrane-impermeable MTS derivatives, presumably due to the increased availability of MTSEA-biotin by masking of the cysteines of other proteins. Together, these results suggest that the subregion of PS1 from G78 through I100 penetrates the membrane as TMD1, and that the N-terminal region of TMD1 sits in a hydrophilic, but sterically hindered, environment.

Cross-linking experiments using MTS cross-linkers

We have previously shown that the amino acid residues in TMD6 are located in proximity to those in TMD7 and TMD9, which are collectively involved in the formation of the catalytic pore, by cross-linking experiments (Sato et al., 2006, 2008). To investigate whether TMD1 also is facing to the catalytic pore, we performed cross-linking experiments using MTS cross-linkers. M2M, M3M, M4M, M6M, M8M, M11M, M14M, and M17M are sulfhydryl-to-sulfhydryl cross-linking reagents with spacer arms 5.2, 6.5, 7.8, 10.4, 13.0, 16.9, 20.8, and 24.7 Å long, respectively (Loo and Clarke, 2001). No cross-linked products were observed by coincubation with any MTS cross-linker in samples from cells expressing single-Cys mt PS1 (supplemental Fig. 3, available at www.jneurosci.org as supplemental material), in accordance with previous findings (Sato et al., 2006, 2008). We next generated double-Cys mutant PS1 bearing a pair of Cys, one located within TMD1 (M84C, V89C, or V94C) and the other in CTF, in positions previously shown to be located within the catalytic pore (i.e., L383C in TMD7, I387C, and L435C in PAL motif at TMD9) (for a summary, see Table 1). All double-Cys mt PS1 showed the γ-secretase activity (supplemental Fig. 4, available at www.jneurosci.org as supplemental material). Coincubation of all double-Cys mt PS1 (except V94C/I387C) with MTS cross-linkers yielded a novel band migrating closely to the PS1 holoprotein (Fig. 4; supplemental Fig. 5, available at www.jneurosci.org as supplemental material). Anti-PS1 NTF and CTF antibodies gave the same results, suggesting that these bands correspond to cross-linked products of NTF and CTF of PS1, in accordance with the previous observations (Sato et al., 2006, 2008). These results indicate that TMD1 faces an identical hydrophilic catalytic pore that is formed by TMD7 and TMD9. Notably, in M84C/L383C, V89C/L383C, and V89C/L435C, cross-linked products were observed by coincubation with M2M harboring a spacer arm 5.2 Å in length. In contrast, other double-Cys mt PS1 required longer cross-linkers (i.e., M8M with spacer arm of 13.0 Å in M84C/I387C, V89C/I387C, and V94C/L383C; M11M with spacer arm of 16.9 Å in M84C/L435C). Thus, M84 and V89 are predicted to be located in close proximity to the catalytic center, as L383 is located in only two amino acids away from D385, the latter being one of the catalytic aspartates of PS1. These results suggest that the N-terminal region of TMD1 participates in the formation of the hydrophilic structure that resides within the cytosolic side of the catalytic pore.

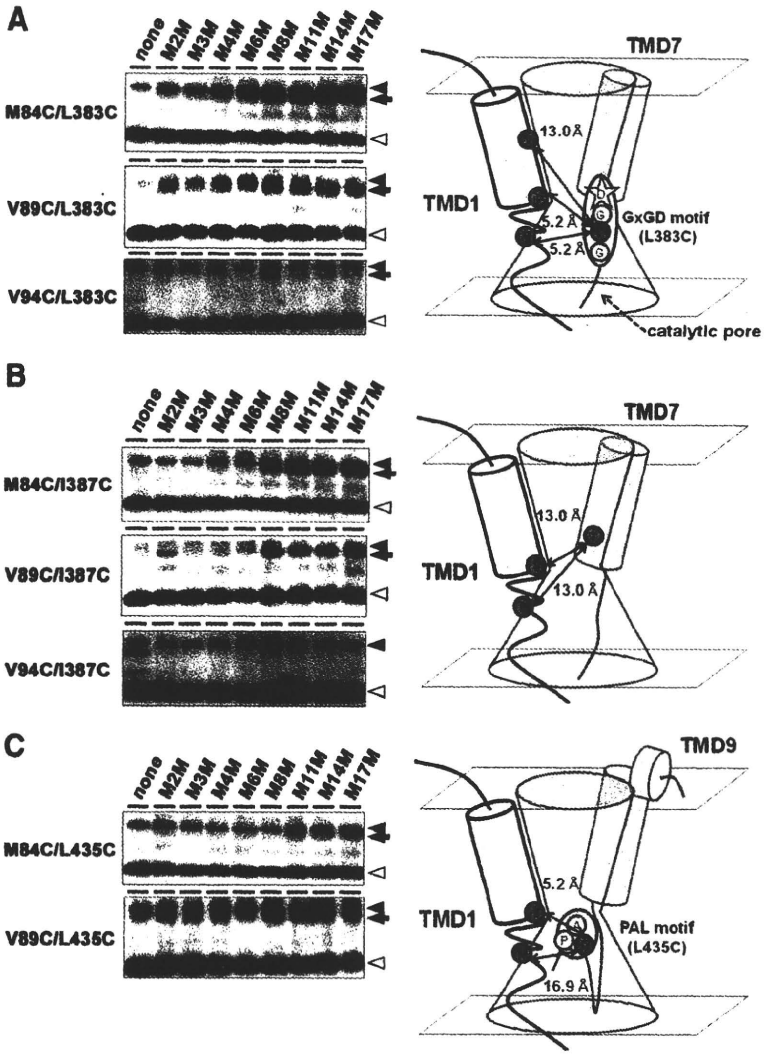

Figure 4. Cross-linking experiments of TMD1 and C-terminal residues using MTS cross-linkers. ***A–C***, Microsome fractions from DKO cells expressing the double-Cys mt carrying one Cys residue at TMD1 and the other at L383C (***A***), I387C (***B***), or L435C (***C***) were incubated with MTS cross-linkers and were separated in SDS-PAGE under nonreducing conditions. Immunoblot analysis was performed using anti-$PS1_{NT}$ antibody. Locations of Cys substitution are shown at the left side of the panel. PS1 FL, NTF, and cross-linked product (NTF-CTF heterodimer) are shown by black arrowheads, white arrowheads, and black arrows, respectively. The predicted maximum lengths between the two residues are indicated in the schematic illustrations at the right side.

Effects of γ-secretase inhibitors on the MTS labeling of TMD1 and Aβ secretion

Next, we examined the effects of three GSIs (i.e., L-685,458, pep15, and DAPT) that have been well characterized functionally and belong to distinct classes of inhibitors on the accessibility of MTSEA-biotin to substituted Cys residues as previously described (Sato et al., 2006, 2008). L-685,458 is a transition-state analog-type GSI that targets the catalytic aspartates, and directly binds NTF and CTF of PS1 (Li et al., 2000; Shearman et al., 2000). Pep15 is a helical peptide-based GSI mimicking the TMD structure, which also binds to PS1 NTF and CTF but does not share the binding site with the transition-state analog inhibitors (Das et al.,

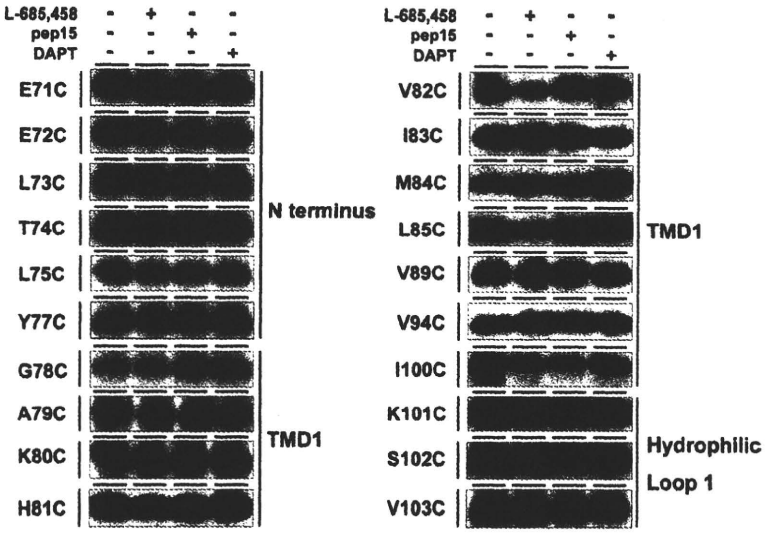

Figure 5. Labeling competition by γ-secretase inhibitors. Biotin labeling of single-Cys mt PS1 was performed after preincubation with L-685,458, pep15, or DAPT. Locations and predicted topology of Cys mutations are shown at left and right, respectively.

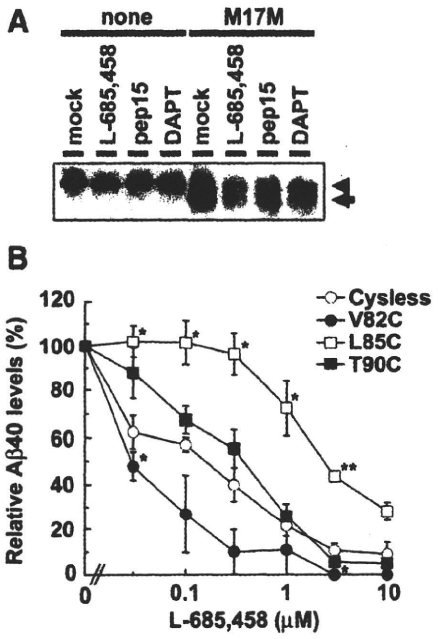

Figure 6. Effect of γ-secretase inhibitors on cross-linking and γ-secretase activity in Cys mt PS1. *A*, Cross-linking experiment on PS1 harboring double Cys (M84C and I387C) was performed in the presence of L-685,458, pep15 or DAPT. Immunoblot analysis was performed using anti-$PS1_{NT}$ antibody. PS1 FL and cross-linked product (NTF-CTF heterodimer) are shown by black arrowheads and black arrows, respectively. *B*, Inhibitory effect of L-685,458 on the Aβ40 secretion from DKO cells expressing PS1/Cys(−), V82C, L85C, or T90C. Secreted Aβ40 in conditioned media was quantitated by ELISA [$n = 3$; mean ± SE; $^*p < 0.05$, $^{**}p < 0.01$ compared with PS1/Cys(−)].

2003; Kornilova et al., 2005). A dipeptidic inhibitor, DAPT binds to PS1 CTF at a site distinct from, but overlapping with, those of transition-state analogs and helical peptides (Kornilova et al., 2003, 2005; Morohashi et al., 2006). Surprisingly, all three GSIs augmented the labeling of G78C, suggesting that the water accessibility of G78 is increased in an enzymatically inactive γ-secretase. In sharp contrast, the labeling of I100C was decreased by preincubation with one or the other of GSIs. The reciprocal changes in the water accessibility of G78 and I100, which are presumed to be located at the cytoplasmic and luminal borders of TMD1, respectively, upon incubation with the GSIs, may implicate a vertical movement of TMD1 depending on the enzymatically active or inactive states of PS1. In addition, the accessibility of MTSEA-biotin to V82C and L85C was substantially decreased specifically with L-685,458 (Fig. 5), similarly to A246C, L381C, and Cys mutants around the PAL motif (Sato et al., 2006, 2008). Together with the data from cross-linking experiments, these results suggest that L-685,458 occupies the hydrophilic space formed by TMDs 1, 7, and 9 at the cytosolic side of the pore, and that V82 and L85 are involved in the binding of L-685,458. To further test this possibility, we examined the effects of GSIs on the cross-linking of M84C/I387C. The biotinylation of I387C single Cys mutant PS1 was not affected by preincubation of GSIs, as in M84C single Cys mutant (Fig. 5) (Sato et al., 2006). However, the amount of cross-linked products in M84C/I387C was significantly decreased by preincubation with L-685,458 (Fig. 6*A*). We have shown that L-685,458, which targets the catalytic site as well as the subsites of γ-secretase (Li et al., 2000), specifically affected the labeling of residues near these cross-linked residues [i.e., V82 and L85 (Fig. 5); L381 and L383 (Sato et al., 2006)]. Thus, the binding of L-685,458 might sterically interrupt the accessibility of MTS cross-linker to PS1 by occupation of the hydrophilic pore, of which the cytosolic side of TMD1 is involved in its formation. Interestingly, preincubation by DAPT or pep15 also substantially decreased the levels of cross-linked products. The binding sites of these GSIs are overlapped, but different, from those of the transition-state analog (Das et al., 2003; Kornilova et al., 2003, 2005; Morohashi et al., 2006), and the biotinylation of the residues in TMD1 was not affected by either DAPT or pep15. Collectively, these data support the notion that DAPT and pep15 harbor the allosteric effects on the TMD1. Finally, we examined the inhibitory potency of L-685,458 against Cys mutant of TMD1. The inhibitory potency of L-685,458 in DKO cells expressing V82C was significantly augmented, whereas that in L85C was decreased, compared with that in PS1/Cys(−). In contrast, T90C, which was not labeled by MTSEA-biotin, showed a similar response to L-685,458 compared with PS1/Cys(−) (Fig. 6*B*), suggesting that the amino acid substitution at V82 or L85 significantly altered the structure of the binding site for L-685,458. Collectively, these observations suggest that V82 and L85 at the N-terminal region of TMD1 comprise a part of the subsite for γ-secretase within the catalytic pore.

Discussion

The structure of TMD1 of PS1 in an enzymatically active γ-secretase complex

Here, we show for the first time that TMD1 of PS1, composed of residues G78 to I100, is located in proximity to TMD7 and TMD9, and faces the catalytic pore of γ-secretase within the lipid bilayer (Fig. 7*A*). Amino acid alignment of PS orthologs reveals that most of the PS family members harbor a highly conserved proline–valine (PV) residues (at 88th and 89th positions in human PS1) at the center of the putative TMD1 (supplemental Fig.

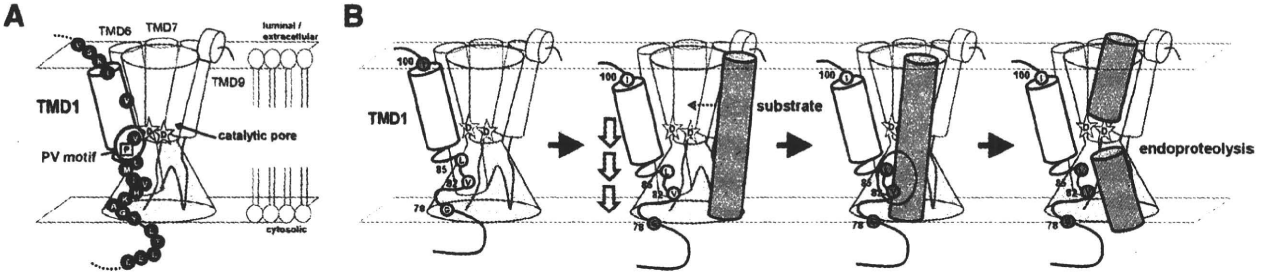

Figure 7. Structure and function of TMD1 of PS1 in relation to the γ-cleavage. ***A***, Summary of SCAM analysis and a schematic depiction of the configuration of the TMD1 in relevance to the catalytic pore. Proline 88 is indicated by a square. Cys mutants that were labeled by MTSEA-biotin are shown in circle frames. Residues whose labeling was competed for by MTS-TEAE, MTSES, and MTSET are shown by blue circles. Residues whose labeling was competed for by MTSES or MTSET, but not by MTS-TEAE, are indicated by sky-blue circles. Residues whose labeling was not affected by any charged residues are indicated by purple circles. ***B***, Schematic presentation of the functional role of TMD1 in the γ-cleavage process. Binding of the substrate to the initial substrate binding site causes the piston movement (purple arrows) and changes the microenvironment of G78 and I100 at the membrane border (indicated by gray and blue circles as decreased and increased hydrophilicity, respectively). A substrate is recognized by the subsite in the catalytic pore (purple oval) where V82 and L85 at N-terminal region of TMD1 (orange circles) are involved in its formation.

6, available at www.jneurosci.org as supplemental material). We showed that V89C was accessible to MTSEA-biotin from the cytosolic side, and cross-linkable to residues of the catalytic GxGD and PAL motifs, suggesting that the PV motif in TMD1 is located in proximity to the catalytic center. Transmembrane helix kinks commonly occur at proline residues (von Heijne, 1991). It has also been suggested that mutations of the N- and C-terminal regions of TMD1 differentially affected the PS endoproteolysis and the γ-secretase activity (Brunkan et al., 2005). Consistently, we showed that N- and C-terminal portions of TMD1 divided by the PV motif exhibit distinct labeling patters by MTS reagent: consecutive residues from G78 to L85 were accessible to MTSEA-biotin, whereas V94C was the only labeled residue in the C-terminal region of TMD1. We speculate that the conserved proline 88 produces a kink in a way to separate TMD1 into two functional regions.

We thoroughly analyzed the hydrophilic environment around TMD1 and found that the cytosolic N-terminal region of the TMD1 may constitute the catalytic structure. Consecutive residues from E71C to Y77C are reactive in microsomes with all charged MTS reagents, including charged bulky MTS-TEAE, indicating that the most N-terminal region of PS1 in a functional state is oriented to the cytosol as previously speculated (Doan et al., 1996). However, the labeling of consecutive residues from G78C to H81C, I83C, and M84C was competed with MTSES or MTSET, but not with MTS-TEAE, suggesting that they lie within a narrower hydrophilic environment. The predicted sizes of the head group of MTSET and MTS-TEAE are 5.8 and 8.0 Å, respectively, possibly reflecting the size of the hydrophilic environment around each modified residue. However, the successive pattern of labeling suggests that this region is not embedded in the lipid bilayer in an α-helical structure. This is highly reminiscent of the pattern of biotinylation of the cytosolic side of TMD7, which we interpreted as a "catalytic plug" structure hung in a hydrophilic pore (Sato et al., 2006). Different competition profile (i.e., competed with MTSES and MTSET in TMD1, but not in TMD7) would reflect the heterogeneity of the hydrophilic milieu within the pore. We speculate that the residues in TMD1 with which MTS-TEAE are unreactive (i.e., G78 to L85) form a hydrophilic structure at the membrane interface of the pore. In addition, M84 was cross-linked to L383 at GxGD motif and L435 at PAL motif. Moreover, the labeling of V82C and L85C was, as in Cys mutants of the GxGD motif, specifically decreased by preincubation with L-685,458 (Fig. 5), and these mutants exhibited an altered sensitivity to L-685,458 (Fig. 6*B*). These data suggest that these residues play a critical role in the γ-secretase activity as a subsite that is involved in substrate recognition during endoproteolysis, although an allosteric effect of L-685,458 on the biotinylation cannot be fully excluded. Collectively, these data support the notion that the cytosolic regions of TMDs 1, 7, and 9 are located in close proximity to each other and may cooperatively function as the catalytic plug.

In contrast to the N-terminal half, most residues in the C-terminal half of TMD1 were hydrophobic: only V94 was water accessible with restrictions and cross-linked with L383. However, no GSIs affected the water accessibility of V94C, suggesting that V94 directly faces the catalytic pore as a part of the pore wall, but do not participate in the formation of a subsite. Notably, the Cys substitution of V96, located at the opposite side of V94 in an α-helical model, caused a loss of protein expression. Consistently, TMD1 is involved in the stabilization of the γ-secretase after the complex assembly is completed (Brunkan et al., 2005; Watanabe et al., 2010). Moreover, amino acid alignment also revealed that V96 is highly conserved from plants to mammals (supplemental Fig. 6, available at www.jneurosci.org as supplemental material). Thus, we speculate that the C-terminal region of TMD1 is an essential domain for maintaining the integrity of PS1 structure via hydrophobic interactions with other TMDs. The observation that C92 in TMD1 was cross-linked with C410 or C419 in TMD8, the latter being totally embedded within the lipid bilayer (Sato et al., 2008), by oxidation-mediated cross-linking (Kornilova et al., 2006), supports this view.

We further characterized the unique feature of the catalytic pore in γ-secretase that has not been observed in other I-CLiPs. We previously reported that the extracellularly accessible L250 in TMD6 was cross-linkable with L435 at the PAL motif that is accessible only from the cytosolic side (Sato et al., 2008). In this study, again, MTS cross-linkers were able to connect the residues accessible only from the cytosol with those from the extracellular/luminal side (i.e., M84C/I387C, V89C/I387C, and V94C/L383C) (Fig. 4). These data indicate that the catalytic pore has a connected structure through the cytosolic and extracellular/luminal sides, as suggested by the single particle analysis of the purified enzyme (Lazarov et al., 2006; Ogura et al., 2006; Osenkowski et al., 2009). This is a unique feature specific to γ-secretase/PS, since the resolved structures of other I-CLiPs (i.e., rhomboid and S2P) exhibit water-including crevasses facing only the extracellular or the cytosolic sides, respectively (Urban and Shi, 2008). The γ-secretase cleaves its substrates at multiple sites with a low sequence specificity (Qi-Takahara et al., 2005; Hemming et al.,

2008), whereas other I-CLiPs generally attack a single site in a sequence-specific manner (Ye et al., 2000; Urban and Wolfe, 2005). It is interesting to speculate that the pore structure is related to the multistep, as well as multisite, γ-secretase-mediated cleavage process.

Implications for the mechanism of intramembrane proteolysis

A previous study has implicated TMD1 in the substrate binding of γ-secretase (Annaert et al., 2001). Photoaffinity labeling and cross-competition experiments have suggested that the substrate-mimic helical peptides target the initial substrate-binding site in PS, which is predicted to be distinct from the catalytic site (Das et al., 2003; Kornilova et al., 2005; Imamura et al., 2009). What, then, is the role of TMD1 in the substrate binding? In this study, however, we failed to detect any specific effects of pep15 on the labeling of TMD1 residues. Rather, competition experiments suggested that TMD1 faces the catalytic pore and functions as a subsite. Notably, Cys substitution of F86 caused an almost complete loss of Aβ generation as well as E-cadherin cleavage, whereas the Notch-cleaving activity was retained in this mutant (supplemental Figs. 1, 7, available at www.jneurosci.org as supplemental material), suggesting that TMD1 plays some role in substrate selection. Nonetheless, we cannot exclude the possibility that TMD1 is directly involved in the substrate binding, in which TMD–TMD interactions at a hydrophobic interface are required, since SCAM analysis using the hydrophilic MTS reagent is unable to detect the hydrophobic interactions.

We raise the possibility that TMD1 dynamically moves in a vertical direction upon substrate binding. We showed that GSIs augmented the hydrophilicity of G78 located at the cytoplasm–membrane border of TMD1. Simultaneously, all three GSIs significantly decreased the water accessibility of I100C, which is positioned at the extracellular membrane interface of TMD1. Altogether, these changes in the labeling pattern suggest that GSIs induced a vertical motion of TMD1 toward the cytosolic side in an allosteric manner. Binding of transition-state analog-type GSIs was shown to stabilize the substrate–PS interaction at the initial substrate binding site, the target of the helical peptide-type GSIs (Esler et al., 2002). These findings may suggest that the vertical motion caused by GSIs was elicited by the occupancy of the initial substrate binding site. Similar motion in TMD caused by ligand binding has been documented as "piston movement" in integrins, bacterial chemoreceptors, β2-adrenergic receptor, and Ca^{2+}-ATPase pump (Williams et al., 1994; Møller et al., 2005; Spijker et al., 2006; Hazelbauer and Lai, 2010). Also, changes in membrane potential trigger a similar motion of TMD in voltage-dependent potassium channels (Gandhi et al., 2003). To our knowledge, this is the first biochemical indication of a motion of PS1 in a membrane-embedded, functional state (for a summary, see Fig. 7*B*).

In sum, we have revealed that TMD1 is a functional component of the catalytic pore structure of the γ-secretase and suggested the dynamic motion of TMD1 during the intramembrane-cleaving process. However, it is unclear whether this motion is a dynamic process correlated with endoproteolysis, and it remains possible that GSIs affect the water accessibility of these residues by an independent mechanism. Nonetheless, further integrated analysis (i.e., molecular dynamics simulation with lipid molecule), in addition to conventional structural analysis of PS at a higher resolution, will provide crucial information for the rational design of GSIs for AD treatment.

References

Annaert WG, Esselens C, Baert V, Boeve C, Snellings G, Cupers P, Craessaerts K, De Strooper B (2001) Interaction with telencephalin and the amyloid precursor protein predicts a ring structure for presenilins. Neuron 32:579–589.

Brunkan AL, Martinez M, Wang J, Walker ES, Beher D, Shearman MS, Goate AM (2005) Two domains within the first putative transmembrane domain of presenilin 1 differentially influence presenilinase and γ-secretase activity. J Neurochem 94:1315–1328.

Das C, Berezovska O, Diehl TS, Genet C, Buldyrev I, Tsai JY, Hyman BT, Wolfe MS (2003) Designed helical peptides inhibit an intramembrane protease. J Am Chem Soc 125:11794–11795.

De Strooper B, Vassar R, Golde T (2010) The secretases: enzymes with therapeutic potential in Alzheimer disease. Nat Rev Neurol 6:99–107.

Doan A, Thinakaran G, Borchelt DR, Slunt HH, Ratovitsky T, Podlisny M, Selkoe DJ, Seeger M, Gandy SE, Price DL, Sisodia SS (1996) Protein topology of presenilin 1. Neuron 17:1023–1030.

Dovey HF, John V, Anderson JP, Chen LZ, de Saint Andrieu P, Fang LY, Freedman SB, Folmer B, Goldbach E, Holsztynska EJ, Hu KL, Johnson-Wood KL, Kennedy SL, Kholodenko D, Knops JE, Latimer LH, Lee M, Liao Z, Lieberburg IM, Motter RN, et al. (2001) Functional γ-secretase inhibitors reduce β-amyloid peptide levels in brain. J Neurochem 76:173–181.

Esler WP, Kimberly WT, Ostaszewski BL, Ye W, Diehl TS, Selkoe DJ, Wolfe MS (2002) Activity-dependent isolation of the presenilin-γ-secretase complex reveals nicastrin and a γ substrate. Proc Natl Acad Sci U S A 99:2720–2725.

Fuwa H, Takahashi Y, Konno Y, Watanabe N, Miyashita H, Sasaki M, Natsugari H, Kan T, Fukuyama T, Tomita T, Iwatsubo T (2007) Divergent synthesis of multifunctional molecular probes to elucidate the enzyme specificity of dipeptidic γ-secretase inhibitors. ACS Chem Biol 2:408–418.

Gandhi CS, Clark E, Loots E, Pralle A, Isacoff EY (2003) The orientation and molecular movement of a K(+) channel voltage-sensing domain. Neuron 40:515–525.

Haass C, Selkoe DJ (2007) Soluble protein oligomers in neurodegeneration: lessons from the Alzheimer's amyloid β-peptide. Nat Rev Mol Cell Biol 8:101–112.

Hayashi I, Urano Y, Fukuda R, Isoo N, Kodama T, Hamakubo T, Tomita T, Iwatsubo T (2004) Selective reconstitution and recovery of functional γ-secretase complex on budded baculovirus particles. J Biol Chem 279:38040–38046.

Hazelbauer GL, Lai WC (2010) Bacterial chemoreceptors: providing enhanced features to two-component signaling. Curr Opin Microbiol 13:124–132.

Hemming ML, Elias JE, Gygi SP, Selkoe DJ (2008) Proteomic profiling of γ-secretase substrates and mapping of substrate requirements. PLoS Biol 6:e257.

Herreman A, Serneels L, Annaert W, Collen D, Schoonjans L, De Strooper B (2000) Total inactivation of γ-secretase activity in presenilin-deficient embryonic stem cells. Nat Cell Biol 2:461–462.

Imamura Y, Watanabe N, Umezawa N, Iwatsubo T, Kato N, Tomita T, Higuchi T (2009) Inhibition of γ-secretase activity by helical β-peptide foldamers. J Am Chem Soc 131:7353–7359.

Isoo N, Sato C, Miyashita H, Shinohara M, Takasugi N, Morohashi Y, Tsuji S, Tomita T, Iwatsubo T (2007) Aβ42 overproduction associated with structural changes in the catalytic pore of γ-secretase: common effects of Pen-2 N-terminal elongation and fenofibrate. J Biol Chem 282:12388–12396.

Iwatsubo T, Odaka A, Suzuki N, Mizusawa H, Nukina N, Ihara Y (1994) Visualization of Aβ42(43) and Aβ40 in senile plaques with end-specific Aβ-monoclonals: Evidence that an initially deposited species is Aβ42(43). Neuron 13:45–53.

Kaback HR, Sahin-Tóth M, Weinglass AB (2001) The kamikaze approach to membrane transport. Nat Rev Mol Cell Biol 2:610–620.

Kan T, Tominari Y, Rikimaru K, Morohashi Y, Natsugari H, Tomita T, Iwatsubo T, Fukuyama T (2004) Parallel synthesis of DAPT derivatives and their γ-secretase-inhibitory activity. Bioorg Med Chem Lett 14:1983–1985.

Karlin A, Akabas MH (1998) Substituted-cysteine accessibility method. Methods Enzymol 293:123–145.

Kitamura T, Koshino Y, Shibata F, Oki T, Nakajima H, Nosaka T, Kumagai H

(2003) Retrovirus-mediated gene transfer and expression cloning: powerful tools in functional genomics. Exp Hematol 31:1007–1014.

Kopan R, Schroeter EH, Weintraub H, Nye JS (1996) Signal transduction by activated mNotch: importance of proteolytic processing and its regulation by the extracellular domain. Proc Natl Acad Sci U S A 93:1683–1688.

Kornilova AY, Das C, Wolfe MS (2003) Differential effects of inhibitors on the γ-secretase complex. Mechanistic implications. J Biol Chem 278:16470–16473.

Kornilova AY, Bihel F, Das C, Wolfe MS (2005) The initial substrate-binding site of γ-secretase is located on presenilin near the active site. Proc Natl Acad Sci U S A 102:3230–3235.

Kornilova AY, Kim J, Laudon H, Wolfe MS (2006) Deducing the transmembrane domain organization of presenilin-1 in γ-secretase by cysteine disulfide cross-linking. Biochemistry 45:7598–7604.

Lazarov VK, Fraering PC, Ye W, Wolfe MS, Selkoe DJ, Li H (2006) Electron microscopic structure of purified, active γ-secretase reveals an aqueous intramembrane chamber and two pores. Proc Natl Acad Sci U S A 103:6889–6894.

Lehmann S, Chiesa R, Harris DA (1997) Evidence for a six-transmembrane domain structure of presenilin 1. J Biol Chem 272:12047–12051.

Li X, Greenwald I (1996) Membrane topology of the *C. elegans* SEL-12 presenilin. Neuron 17:1015–1021.

Li YM, Xu M, Lai MT, Huang Q, Castro JL, DiMuzio-Mower J, Harrison T, Lellis C, Nadin A, Neduvelil JG, Register RB, Sardana MK, Shearman MS, Smith AL, Shi XP, Yin KC, Shafer JA, Gardell SJ (2000) Photoactivated γ-secretase inhibitors directed to the active site covalently label presenilin 1. Nature 405:689–694.

Loo TW, Clarke DM (2001) Determining the dimensions of the drug-binding domain of human P-glycoprotein using thiol cross-linking compounds as molecular rulers. J Biol Chem 276:36877–36880.

Møller JV, Nissen P, Sørensen TL, le Maire M (2005) Transport mechanism of the sarcoplasmic reticulum Ca^{2+} -ATPase pump. Curr Opin Struct Biol 15:387–393.

Morohashi Y, Kan T, Tominari Y, Fuwa H, Okamura Y, Watanabe N, Sato C, Natsugari H, Fukuyama T, Iwatsubo T, Tomita T (2006) C-terminal fragment (CTF) of presenilin is the molecular target of a dipeptidic γ-secretase-specific inhibitor DAPT (*N*-[*N*-(3,5-difluorophenacetyl)-*L*-alanyl]-*S*-phenylglycine *t*-butyl ester). J Biol Chem 281:14670–14676.

Nakai T, Yamasaki A, Sakaguchi M, Kosaka K, Mihara K, Amaya Y, Miura S (1999) Membrane topology of Alzheimer's disease-related presenilin 1. Evidence for the existence of a molecular species with a seven membrane-spanning and one membrane-embedded structure. J Biol Chem 274:23647–23658.

Ogura T, Mio K, Hayashi I, Miyashita H, Fukuda R, Kopan R, Kodama T, Hamakubo T, Iwatsubo T, Iwastubo T, Tomita T, Sato C (2006) Three-dimensional structure of the γ-secretase complex. Biochem Biophys Res Commun 343:525–534.

Osenkowski P, Li H, Ye W, Li D, Aeschbach L, Fraering PC, Wolfe MS, Selkoe DJ, Li H (2009) Cryoelectron microscopy structure of purified gamma-secretase at 12 angstroms resolution. J Mol Biol 385:642–652.

Qi-Takahara Y, Morishima-Kawashima M, Tanimura Y, Dolios G, Hirotani N, Horikoshi Y, Kametani F, Maeda M, Saido TC, Wang R, Ihara Y (2005) Longer forms of amyloid β protein: implications for the mechanism of intramembrane cleavage by γ-secretase. J Neurosci 25:436–445.

Sato C, Morohashi Y, Tomita T, Iwatsubo T (2006) Structure of the catalytic pore of γ-secretase probed by the accessibility of substituted cysteines. J Neurosci 26:12081–12088.

Sato C, Takagi S, Tomita T, Iwatsubo T (2008) The C-terminal PAL motif and transmembrane domain 9 of presenilin 1 are involved in the formation of the catalytic pore of the γ-secretase. J Neurosci 28:6264–6271.

Shearman MS, Beher D, Clarke EE, Lewis HD, Harrison T, Hunt P, Nadin A, Smith AL, Stevenson G, Castro JL (2000) L-685,458, an aspartyl protease transition state mimic, is a potent inhibitor of amyloid β-protein precursor γ-secretase activity. Biochemistry 39:8698–8704.

Sobhanifar S, Schneider B, Löhr F, Gottstein D, Ikeya T, Mlynarczyk K, Pulawski W, Ghoshdastider U, Kolinski M, Filipek S, Güntert P, Bernhard F, Dötsch V (2010) Structural investigation of the C-terminal catalytic fragment of presenilin 1. Proc Natl Acad Sci U S A 107:9644–9649.

Spijker P, Vaidehi N, Freddolino PL, Hilbers PA, Goddard WA 3rd (2006) Dynamic behavior of fully solvated β2-adrenergic receptor, embedded in the membrane with bound agonist or antagonist. Proc Natl Acad Sci U S A 103:4882–4887.

Takahashi Y, Hayashi I, Tominari Y, Rikimaru K, Morohashi Y, Kan T, Natsugari H, Fukuyama T, Tomita T, Iwatsubo T (2003) Sulindac sulfide is a noncompetitive γ-secretase inhibitor that preferentially reduces Aβ42 generation. J Biol Chem 278:18664–18670.

Takasugi N, Tomita T, Hayashi I, Tsuruoka M, Niimura M, Takahashi Y, Thinakaran G, Iwatsubo T (2003) The role of presenilin cofactors in the γ-secretase complex. Nature 422:438–441.

Thinakaran G, Regard JB, Bouton CM, Harris CL, Price DL, Borchelt DR, Sisodia SS (1998) Stable association of presenilin derivatives and absence of presenilin interactions with APP. Neurobiol Dis 4:438–453.

Tolia A, Chávez-Gutiérrez L, De Strooper B (2006) Contribution of presenilin transmembrane domains 6 and 7 to a water-containing cavity in the γ-secretase complex. J Biol Chem 281:27633–27642.

Tolia A, Horré K, De Strooper B (2008) Transmembrane domain 9 of presenilin determines the dynamic conformation of the catalytic site of γ-secretase. J Biol Chem 283:19793–19803.

Tomita T (2009) Secretase inhibitors and modulators for Alzheimer's disease treatment. Expert Rev Neurother 9:661–679.

Tomita T, Maruyama K, Saido TC, Kume H, Shinozaki K, Tokuhiro S, Capell A, Walter J, Grünberg J, Haass C, Iwatsubo T, Obata K (1997) The presenilin 2 mutation (N141I) linked to familial Alzheimer disease (Volga German families) increases the secretion of amyloid β protein ending at the 42nd (or 43rd) residue. Proc Natl Acad Sci U S A 94:2025–2030.

Tomita T, Tokuhiro S, Hashimoto T, Aiba K, Saido TC, Maruyama K, Iwatsubo T (1998) Molecular dissection of domains in mutant presenilin 2 that mediate overproduction of amyloidogenic forms of amyloid β peptides. Inability of truncated forms of PS2 with familial Alzheimer's disease mutation to increase secretion of Aβ42. J Biol Chem 273:21153–21160.

Tomita T, Takikawa R, Koyama A, Morohashi Y, Takasugi N, Saido TC, Maruyama K, Iwatsubo T (1999) C terminus of presenilin is required for overproduction of amyloidogenic Aβ42 through stabilization and endoproteolysis of presenilin. J Neurosci 19:10627–10634.

Tomita T, Watabiki T, Takikawa R, Morohashi Y, Takasugi N, Kopan R, De Strooper B, Iwatsubo T (2001) The first proline of PALP motif at the C terminus of presenilins is obligatory for stabilization, complex formation, and γ-secretase activities of presenilins. J Biol Chem 276:33273–33281.

Urban S, Shi Y (2008) Core principles of intramembrane proteolysis: comparison of rhomboid and site-2 family proteases. Curr Opin Struct Biol 18:432–441.

Urban S, Wolfe MS (2005) Reconstitution of intramembrane proteolysis in vitro reveals that pure rhomboid is sufficient for catalysis and specificity. Proc Natl Acad Sci U S A 102:1883–1888.

von Heijne G (1991) Proline kinks in transmembrane α-helices. J Mol Biol 218:499–503.

Watanabe N, Tomita T, Sato C, Kitamura T, Morohashi Y, Iwatsubo T (2005) Pen-2 is incorporated into the γ-secretase complex through binding to transmembrane domain 4 of presenilin 1. J Biol Chem 280:41967–41975.

Watanabe N, Takagi S, Tominaga A, Tomita T, Iwatsubo T (2010) Functional analysis of the transmembrane domains of presenilin 1: Participation of transmembrane domains 2 and 6 in the formation of initial substrate-binding site of γ-secretase. J Biol Chem 285:19738–19746

Williams MJ, Hughes PE, O'Toole TE, Ginsberg MH (1994) The inner world of cell adhesion: integrin cytoplasmic domains. Trends Cell Biol 4:109–112.

Wolfe MS, Kopan R (2004) Intramembrane proteolysis: theme and variations. Science 305:1119–1123.

Ye J, Davé UP, Grishin NV, Goldstein JL, Brown MS (2000) Asparagine-proline sequence within membrane-spanning segment of SREBP triggers intramembrane cleavage by site-2 protease. Proc Natl Acad Sci U S A 97:5123–5128.

THE JOURNAL OF BIOLOGICAL CHEMISTRY VOL. 285, NO. 26, pp. 19738–19746, June 25, 2010

Functional Analysis of the Transmembrane Domains of Presenilin 1

*PARTICIPATION OF TRANSMEMBRANE DOMAINS 2 AND 6 IN THE FORMATION OF INITIAL SUBSTRATE-BINDING SITE OF γ-SECRETASE**

Received for publication, January 5, 2010, and in revised form, April 19, 2010 Published, JBC Papers in Press, April 23, 2010, DOI 10.1074/jbc.M110.101287

Naoto Watanabe (渡邊直登)[‡1], Shizuka Takagi (高木穏香)[‡1], Aya Tominaga (富永綾)[‡], Taisuke Tomita (富田泰輔)[‡§2], and Takeshi Iwatsubo (岩坪威)[‡§¶]

From the [‡]Department of Neuropathology and Neuroscience, Graduate School of Pharmaceutical Sciences, and the [¶]Department of Neuropathology, Graduate School of Medicine, The University of Tokyo, Tokyo 113-0033 and [§]Core Research for Evolutional Science and Technology, Japan Science and Technology Corporation, Tokyo 113-0033, Japan

γ-Secretase is a multimeric membrane protein complex composed of presenilin (PS), nicastrin, Aph-1, and Pen-2, which mediates intramembrane proteolysis of a range of type I transmembrane proteins. We previously analyzed the functional roles of the N-terminal transmembrane domains (TMDs) 1–6 of PS1 in the assembly and proteolytic activity of the γ-secretase using a series of TMD-swap PS1 mutants. Here we applied the TMD-swap method to all the TMDs of PS1 for the structure-function analysis of the proteolytic mechanism of γ-secretase. We found that TMD2- or -6-swapped mutant PS1 failed to bind the helical peptide-based, substrate-mimic γ-secretase inhibitor. Cross-linking experiments revealed that both TMD2 and TMD6 of PS1 locate in proximity to the TMD9, the latter being implicated in the initial substrate binding. Taken together, our data suggest that TMD2 and the luminal side of TMD6 are involved in the formation of the initial substrate-binding site of the γ-secretase complex.

γ-Secretase is an unusual aspartic protease that mediates an intramembrane proteolysis of a number of type I transmembrane proteins, including amyloid precursor protein (APP)[3] and Notch receptor (1, 2). A body of evidence revealed that γ-secretase is a high molecular weight (HMW) complex, composed of presenilin (PS), nicastrin (Nct), Aph-1, and Pen-2 (3). Mutations in *PS* genes are linked to the early onset familial Alzheimer disease. Familial Alzheimer disease-linked *PS* mutations influence the processing of APP, leading to an overproduction of amyloid peptide ending at the 42nd residue (Aβ42) that is more prone to forming amyloid deposits. Thus, PS-γ-secretase complex is a plausible therapeutic target for the treatment of Alzheimer disease (1, 2).

PS is a highly conserved polytopic membrane protein with nine transmembrane domains (TMDs), and two conserved aspartates in PS (*i.e.* Asp^{257} in TMD6 and Asp^{385} in TMD7) comprise the catalytic site of the γ-secretase (2). Chemical biological approaches using γ-secretase inhibitors (GSIs) revealed its unusual enzymatic characters; immobilized transition state analogue-type GSIs directly target PS NTF/CTF heterodimer and co-purify with γ-secretase substrates (4). In contrast, designed helical peptide-type GSI binds to PS irrespective of the presence or absence of transition state analogue-type GSIs that occupy the catalytic site (5, 6). These findings strongly suggested that γ-secretase has an "initial substrate-binding site" that is distinct from the catalytic site (2).

During the biosynthetic process of the γ-secretase complex, Nct and Aph-1 form a heterodimeric subcomplex and bind to PS (7, 8). Pen-2 then is assembled to the heterotrimeric complex and triggers the endoproteolysis of PS to generate N- and C-terminal fragments (NTF and CTF), which represent the catalytically active form (3). PS forms a catalytic pore structure in which catalytic aspartates face a hydrophilic environment, enabling the proteolysis of hydrophobic substrates within the lipid bilayer (9–11). However, information regarding the initial substrate-binding site within PS at the molecular level is still lacking. Using TMD-swap mutants of PS1 that are replaced at each one of the TMDs of the NTF with the TMDs of irrelevant proteins, we have shown that all the PS1 TMDs in NTF (*i.e.* TMDs 1–6), except for TMD3, are required for the acquisition of the γ-secretase activity (12). We further showed that PS1 TMD4 represents the direct binding region of Pen-2. Here we further systematically analyzed the TMD-swap mutants of PS1 and revealed the stepwise formation of the functional γ-secretase complex. Notably, we found that TMD2 and the luminal side of TMD6 of PS1 contribute to the formation of the initial substrate-binding site of the γ-secretase complex.

* This work was supported in part by grants-in-aid for young scientists (S) from the Japan Society for the Promotion of Science (JSPS), Scientific Research on Priority Areas "Research on Pathomechanisms of Brain Disorders" from the Ministry of Education, Culture, Sports, Science and Technology (MEXT), by the Targeted Proteins Research Program of the Japan Science and Technology Corporation (JST), and by the Core Research for Evolutional Science and Technology of JST, Japan.

[1] Research fellows of the JSPS.

[2] To whom correspondence should be addressed: Dept. of Neuropathology and Neuroscience, Graduate School of Pharmaceutical Sciences, The University of Tokyo, 7-3-1 Hongo, Bunkyo-ku, Tokyo 113-0033, Japan. Tel.: 81-3-5841-4868; Fax: 81-3-5841-4708; E-mail: taisuke@mol.f.u-tokyo.ac.jp.

[3] The abbreviations used are: APP, β-amyloid precursor protein; Aβ, amyloid β peptide; HMW, high molecular weight; CHAPSO, 3-[(3-cholamidopropyl)-dimethylammonio]-2-hydroxy-1-propanesulfonate; CTF, carboxyl-terminal fragment; NTF, amino-terminal fragment; DKO, *PS1/PS2* double knockout fibroblasts; ELISA, enzyme-linked immunosorbent assay; Nct, nicastrin; mt, mutant; PS, presenilin; TMD, transmembrane domain; WT, wild-type; BN-PAGE, Blue Native-PAGE; SCAM, substituted cysteine-scanning method; NICD, Notch intracellular domain; SPP, signal peptide peptidase; MTS, methanethiosulfonate; GSI, γ-secretase inhibitor.

EXPERIMENTAL PROCEDURES

Plasmid Construction, Cell Culture, Transfection, and Retroviral Infection—cDNAs encoding PS1, APP carrying Swedish mutation (APP_{NL}), and NotchΔE were inserted into pMXs-puro (9, 11–13). cDNAs encoding mutant PS1 were generated by long PCR-based QuikChange™ strategy (Stratagene). All constructs were sequenced using Thermo Sequenase (USB Corp., Cleveland, OH) on an automated sequencer (Li-Cor, Lincoln, NE) (see Table 1). Maintenance of DKO cells, viral packaging in Plat-E cells, retroviral infection, and generation of stable infectant pools were done as described previously (9, 11–14).

Antibodies and Immunochemical Analyses—Anti-G1Nr2, G1L3, and PNT3 antibodies against glutathione *S*-transferase-fused human PS1 N terminus, glutathione *S*-transferase-fused human PS1 loop, or a synthetic peptide corresponding to the N-terminal 26 amino acids of human/mouse Pen-2, respectively, have been previously described (3, 15, 16). Anti-$PS1_{NT}$, anti-PS-C3, and anti-SPP_{ct} antibodies were kindly provided by Drs. G. Thinakaran (University of Chicago, Chicago, IL), A. Takashima (RIKEN, Saitama, Japan), and T. E. Golde (Mayo Clinic, Jacksonville, FL), respectively (17–19). The monoclonal antibody anti-α-tubulin AA4.3 developed by Dr. C. Walsh was obtained from the Developmental Studies Hybridoma Bank developed under the auspices of the NICHD, National Institutes of Health, and maintained by The University of Iowa, Department of Biology, Iowa City, IA. Other antibodies were purchased from Chemicon (anti-PS1 loop (MAB5232)), Cell Signaling Technology (anti-cleaved Notch1 (V1744)), Covance (anti-Aph-1aL (O2C2)), Santa Cruz Biotechnology (anti-Nct (N19)), or Sigma (anti-Nct (N1660)). Membrane fractionation, immunoblot analysis, immunoprecipitation of CHAPSO-solubilized lysates, *in vitro* γ-secretase assay, cycloheximide treatment, trypsin digestion, or quantitation of Aβ by two-site ELISAs using BNT77 as a capture antibody were performed as described previously (3, 8, 9, 11–16, 20).

Blue Native-PAGE (BN-PAGE) Analysis—BN-PAGE was performed according to the manufacturer's protocol (Invitrogen). Briefly, membrane fractions were suspended in Native PAGE™ sample buffer containing 1% digitonin (Wako Biochemicals). The mixtures were centrifuged for 10 min at 15,000 × *g*, and Coomassie Brilliant Blue was added to the supernatant to give a final concentration of 0.25% w/v. NativeMark™ unstained protein standard (Invitrogen) was used as a molecular weight standard. After electrophoresis, the gel was transferred to polyvinylidene difluoride membranes. The membranes were destained briefly in methanol before being incubated with specific antibodies.

Compounds, Photoaffinity Labeling, Substituted Cysteine-scanning Method (SCAM), and Cross-linking Experiments—L-685,458, peptide 11 (pep.11) and pep.11-Bt were purchased from Bachem (Torrance, CA), Ito Life Sciences (Moriya, Japan), and BEX (Tokyo, Japan), respectively. L-852,646 was kindly provided by Dr. Yueming Li (21). All methanethiosulfonate (MTS) reagents (Toronto Research Chemicals) were dissolved in dimethyl sulfoxide (DMSO) at 200 mM prior to use or stored at −80 degree until use. Photoaffinity labeling, SCAM, and cross-linking experiments were performed as described previously (6, 9, 11, 22, 23).

TABLE 1
Amino acid alignment of swapped region in TMD-swap PS1 mutants
Alignments of amino acid sequences of the TMDs of PS1 and CD4 or CLAC-P are shown. Numbers indicate the region for TMD-swap mutant in PS1. Amino acid sequences remained as those of PS1 in TM6mt are underlined.

TM1mt	^{82}VIMLFVPVTLCMVVVVATI^{100}	PS1 TMD1
	^{82}CAVLAALLSVVAVVSCLYL^{100}	CLAC-P
TM2mt	^{135}NAAIMISVIVVMTILLVVLY^{154}	PS1 TMD2
	^{135}ALIVLGGVAGLLLFIGLGIF^{154}	CD4
TM3mt	^{164}AWLIISSLLLLFFFSFIYLG^{183}	PS1 TMD3
	^{164}CAVLAALLSVVAVVSCLYLG^{183}	CLAC-P
TM4mt	^{190}NVAVDYITVALLIWNFGVVGMISI^{213}	PS1 TMD4
	^{190}MALIVLGGVAGLLLFIGLGIFFCV^{213}	CD4
TM5mt	^{219}LRLQQAYLIMISALMALVFI^{238}	PS1 TMD5
	^{219}CAVLAALLSVVAVVSCLYLG^{238}	CLAC-P
TM6mt	^{244}WTAWLILAVISVYDLVAVL^{255}	PS1 TMD6
	^{244}MALIVLGGVAGLYDLVAVL^{255}	CD4/TMD6
TM8mt	^{408}IACFVAILIGLCLTLLLLAIF^{428}	PS1 TMD8
	^{408}MALIVLGGVAGLLLFIGLGIF^{428}	CD4
TM9mt	^{434}ALPISITFGLVFYFATDYLV^{453}	PS1 TMD9
	^{434}CAVLAALLSVVAVVSCLYLG^{453}	CLAC-P

RESULTS

Transmembrane Domains 8 and 9 of Presenilin 1 are Required for the γ-Secretase Activity—We have previously analyzed the functional role(s) of the PS TMDs using TMD-swap mutants (12). We applied this strategy to PS1 CTF and constructed cDNAs encoding PS1 mutants (*i.e.* TM8mt, TM9mt) in which TMD8 (408–428 amino acids) or TMD9 (434–453 amino acids) was replaced with TMDs of functionally unrelated transmembrane proteins, *i.e.* CD4 (type I transmembrane protein) or CLAC-P (type II transmembrane protein), respectively (Table 1). As reported previously, overexpression of wild-type (WT) PS1 in DKO cells resulted in the generation of PS fragments and recovered the levels of mature Nct and the accumulation of Pen-2 (Fig. 1*A*) (12). Both TM8mt and TM9mt also rescued the accumulation of mature Nct and Pen-2, although the level of mature Nct in DKO cells expressing TM8mt was lower than that in cells expressing WT PS1. However, endoproteolysis of TM8mt or TM9mt PS1 was not observed. We next analyzed the γ-secretase activities of the TMD-swap mutants in DKO cells. Unexpectedly, neither TM8mt nor TM9mt recovered the γ-secretase activity to generate NICD or Aβ in cell-based assays (Fig. 1, *B* and *C*). These TMD-swap mutants also displayed no proteolytic activity in *in vitro* assays (data not shown).

To address whether replacement of the PS1 TMDs interferes with the formation of γ-secretase complex, we analyzed the CHAPSO lysates of DKO cells expressing WT or mutant PS1 by co-immunoprecipitation (Fig. 1*D*). Upon overexpression of WT PS1, all other γ-secretase components (*i.e.* Nct, Aph-1aL, and Pen-2) were co-precipitated with WT PS1. In contrast, TM4mt and the C-terminal deletion mutant PS1 that lacks the C-terminal 12 amino acids (*i.e.* PS1/455stop) failed to bind the Pen-2 or Nct-Aph-1 subcomplex, respectively, in accordance with previous reports (12, 24, 25). Notably, all TMD-swap mutants including TM8mt and TM9mt interacted with Nct, Aph-1aL, and Pen-2, indicating that the primary amino acid sequences of TMD8 or -9 are dispensable to the interaction with γ-secretase components. Taken together, these results indicate that the primary structures of PS1 TMD8 and -9 con-

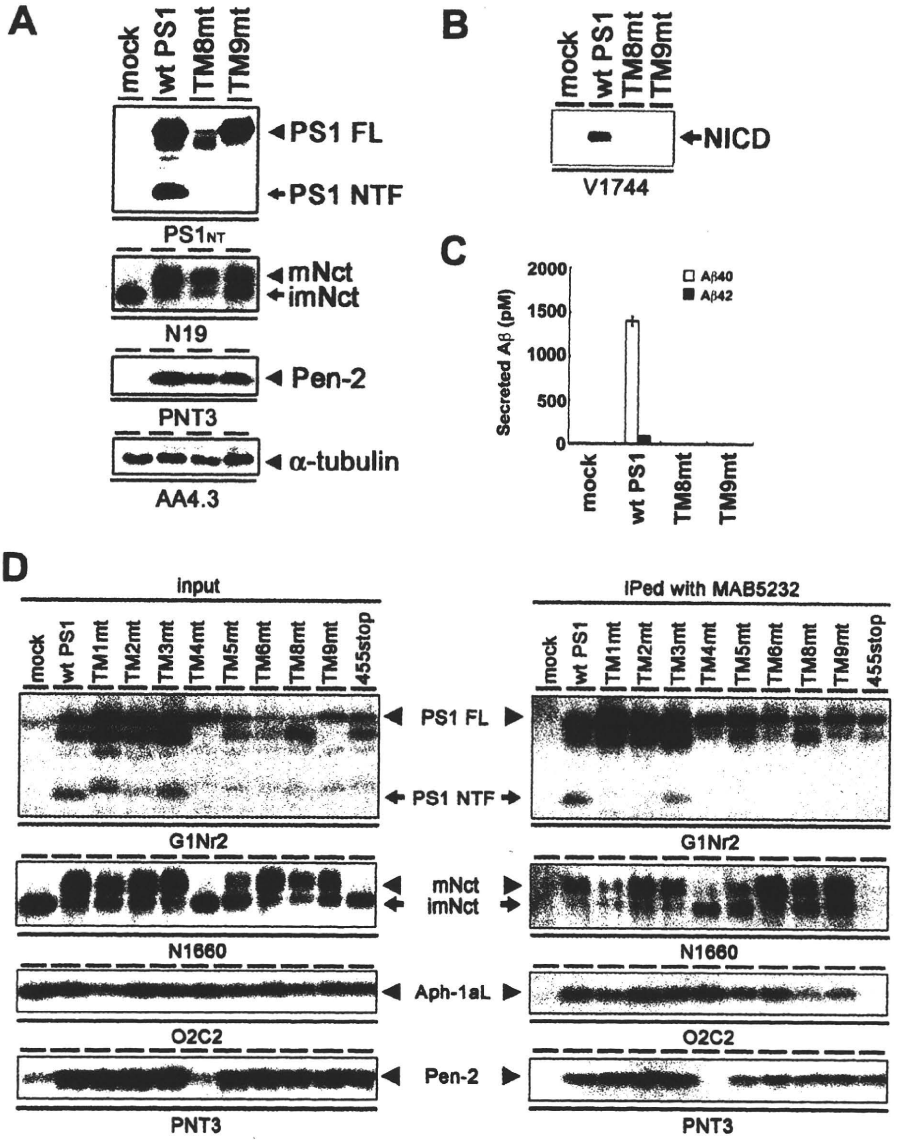

FIGURE 1. **Complementation of maturation of Nct and accumulation of Pen-2 by expression of TM8mt and TM9mt in DKO cells.** *A*, immunoblot analysis of DKO cells stably transfected with WT or mutant PS1 (as indicated above the panel). Cell lysates were analyzed by immunoblotting with each antibody (as indicated below the panel). *FL*, full length; *mNct*, mature nicastrin; *imNct*, immature nicastrin. *B*, immunoblot analysis of the generation of NICD from NotchΔE-stable DKO cells. *C*, sandwich ELISA analysis of secreted Aβ from APP_{NL}-stable DKO cells transiently expressing TMD-swap PS1 mutants. The levels of Aβ40 and Aβ42 are shown by *white* and *black bars*, respectively. *Error bars* indicate S.E. *D*, co-immunoprecipitation analysis of 1% CHAPSO-solubilized fractions prepared from DKO cells transiently transfected with WT or mutant PS1. Soluble fractions were precipitated (*IPed*) by MAB5232 and then analyzed by immunoblotting with each antibody as indicated below the panel.

tribute to the acquisition of the conformation of active γ-secretase or its enzymatic activity but not to the interactions with other essential components of γ-secretase.

Intramolecular Complementation Assay by Co-expression of NTF and CTF Individually in DKO Cells—Several lines of evidence suggest that the biologically active form of PS is the NTF/CTF heterodimer, although the functional significance of endoproteolysis remains to be elucidated. To ask whether ineffective endoproteolysis inhibited the proteolytic activity of the TMD-swap PS mutant, we further examined the effects of TMD-swaps in an intramolecular complementation analysis by co-expression of NTF and CTF in DKO cells (Fig. 2*A*). The level of protein expression of TM4mt NTF was relatively low, supporting the notion that the interaction of PS1 with Pen-2 is involved in the stabilization of the γ-secretase complex (12, 26) (see below). As reported, expression of WT NTF and WT CTF from separate vectors was able to restore the γ-secretase activity (25) (Fig. 2*B*). Interestingly, co-expression of TM3mt NTF with WT CTF improved the total Aβ-generating as well as the NICD-generating activities of γ-secretase more than those in cells expressing the TM3mt holoprotein (12). In addition, TM3mt showed a significant decrease in the production of Aβ40 and a reciprocal increase in that of Aβ42, respectively. Of note, the same trend in the generation of Aβ40 and Aβ42 had been observed in holoprotein-based TM3mt PS1 (12). In fact, the total levels of Aβ and NICD were almost similar to those in cells expressing WT NTF/WT CTF ($n = 3, p = 0.12$ (for Aβ) and $p = 0.30$ (for NICD) by Student's t test). This result suggests that the TMD3 of PS1 harbors as yet unknown function to promote the γ-secretase activity after endoproteolysis regardless of the substrates. Further analysis on the role of TMD3 on substrates other than APP and Notch would be required. Intriguingly, some residues on TMD3 have been implicated in the determination of PS1/PS2 specificity of a subset of the γ-secretase inhibitors (26). Nevertheless, these data support the idea that TMD3 is involved in the acquisition of proper cleavage activity of the γ-secretase after the assembly of the complex. However, none of the other TMD-swap mutants expressed in an endoproteolyzed form rescued any γ-secretase activity, suggesting that the structures of each of these TMDs of PS1, other than TMD4, are indispensable to the acquisition of γ-secretase activity, independently from their roles in PS endoproteolysis.

TMD1, -5, -8, and -9 Are Required for the Stability, but Not the Formation, of the HMW Complex—During the assembly of the functional γ-secretase complex, Nct acquires resistance against trypsin and undergoes the complex-type *N*-glycosylation (27). These posttranslational modifications represent conformational maturation of the extracellular domain of Nct and

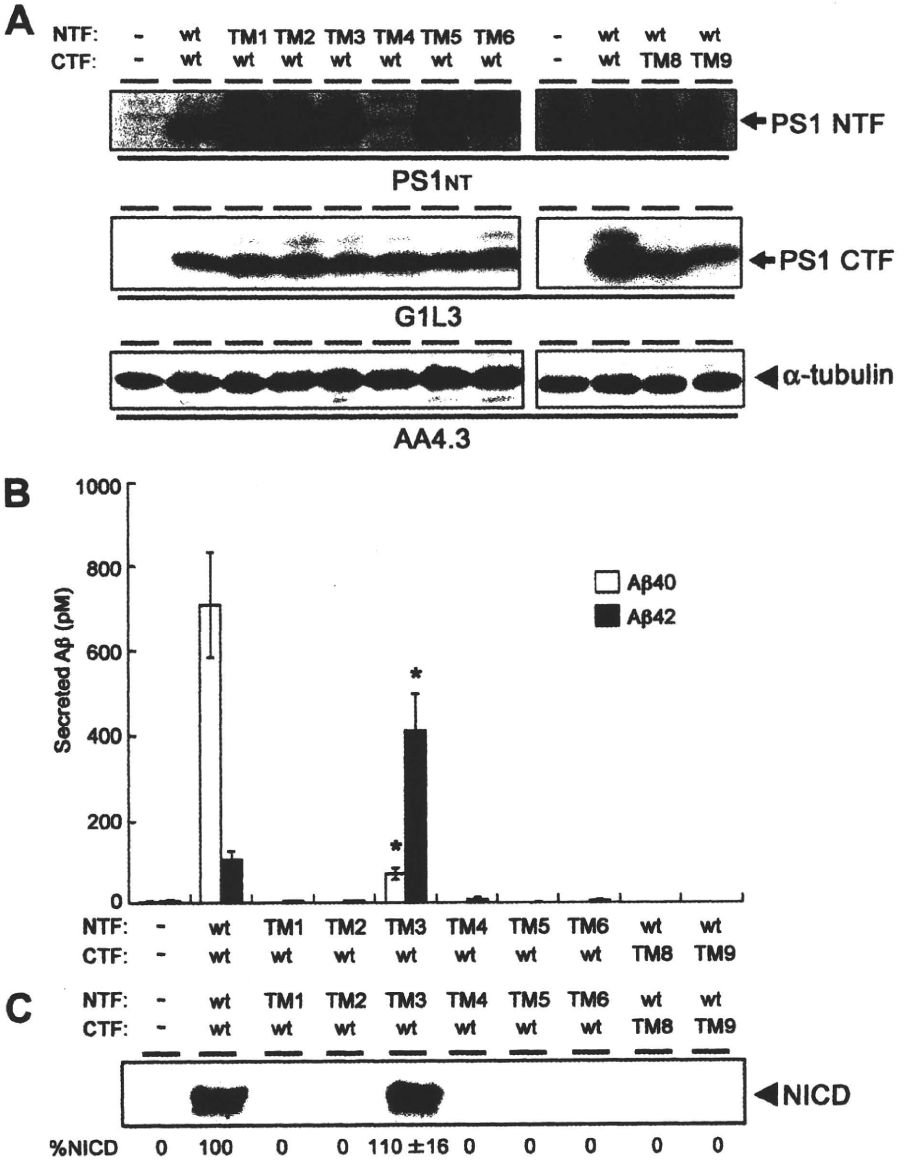

FIGURE 2. **Intramolecular complementation analysis in DKO cells.** *A*, immunoblot analysis of DKO cells transiently co-expressing NTF and CTF of PS1. *B*, sandwich ELISA analysis of secreted Aβ from APP_{NL}-stable DKO cells transiently co-expressing mutant NTFs and CTFs. The levels of Aβ40 and Aβ42 are shown by *white* and *black bars*, respectively. TM3mt exhibited a significantly decreased Aβ40 activity and increased Aβ42-generating activities (*, statistically significant ($n = 3, p < 0.001$) when compared with those in cells co-expressing WT NTF/WT CTF by Student's *t* test). *Error bars* indicate S.E. *C*, immunoblot analysis of the generation of NICD from NotchΔE-stable DKO cells using anti-V1744 antibody. *Numbers* shown below each lane denote the relative band intensities of NICD (%, $n = 3$) when compared with those in cells co-expressing WT NTF/WT CTF.

the proper trafficking of the γ-secretase complex (28–31). Mature Nct proteins were detected in all TMD-swap-expressing cell lysates, except for TM4mt, suggesting that the trafficking of the γ-secretase complex was not significantly altered by the swapping of TMDs (Fig. 3). Moreover, the maturated form of Nct proteins expressed with TMD-swap PS1 acquired the resistance against trypsin treatment independent of the PS1 genotype. However, the levels of mature Nct were significantly lower in cells expressing TM1mt, TM5mt TM8mt, and TM9mt PS1 when compared with WT PS1. Altogether, the maturation of Nct was unaffected by TMD-swap mutation in PS1 TMDs, except for the TM4mt.

The formation of stabilized HMW complex containing PS is tightly related to its enzymatic function (15, 18). Upon BN-PAGE analysis, all components of the γ-secretase complex were detected at the position of the HMW complex with an apparent molecular mass of 440 kDa (Fig. 4*A*). We used the endogenous signal peptide peptidase (SPP) as a loading control, which was mainly detected as a 200-kDa complex irrespective of the overexpression of PS1.[4] Mutant PS1 carrying M292D, D257A, or D385A mutation was also detected as the ~440-kDa HMW complex, suggesting that the HMW complex formation was independent from the endoproteolysis or the catalytic activity of PS1 (Fig. 4*B*). Consistent with the results of the immunoprecipitation assay, all TMD-swap PS1 mutants were also detected as the HMW complex together with other γ-secretase components. Notably, TM4mt was detected as an ~440-kDa complex, too, indicating that Pen-2 is dispensable for the HMW complex formation. In good agreement with our previous result that TM4mt was unstable (12), the amount of the TM4mt-containing HMW complex was smaller than that of WT PS1. In addition, the steady state levels of TM1mt-, TM5mt-, TM8mt-, or TM9mt-containing HMW complex were significantly lower than that of the HMW complex containing WT PS1. To further analyze the effects of swap of TMDs on the γ-secretase complex, we examined the stability of the HMW complex by cycloheximide treatment. Complex containing WT PS1 was highly stable at the chase of 12 h (Fig. 5*A*). In contrast, TM1mt-, TM4mt-, TM5mt-, TM8mt-, or TM9mt-containing HMW complexes were rapidly degraded (Fig. 5*B*), whereas those containing TM2mt, TM3mt, or TM6mt were highly stabilized similarly to that containing WT PS1. We then examined the major conformational change of TMD-swap PS1 mutants by trypsin digestion (Fig. 6). Unexpectedly, the patterns of digested bands of the

[4] N. Watanabe, T. Iwatsubo, and T. Tomita, unpublished data.

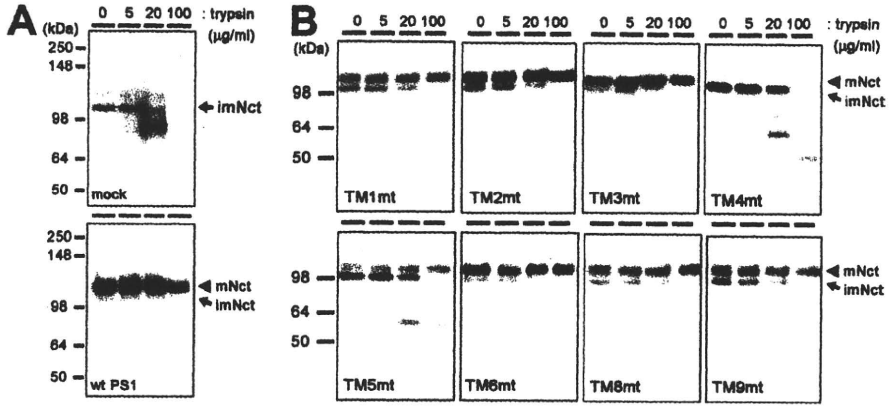

FIGURE 3. **Trypsin digestion of Nct polypeptides in DKO cells expressing TMD-swap PS1 mutants.** 1% CHAPSO-solubilized lysates prepared from DKO cells transiently transfected with WT PS1 (*A*) or TMD-swap PS1 mutants (*B*) were divided into four samples and incubated with trypsin as indicated by concentrations above the panels and analyzed by immunoblotting using anti-Nct antibody (N1660). *imNct*, immature nicastrin; *mNct*, mature nicastrin.

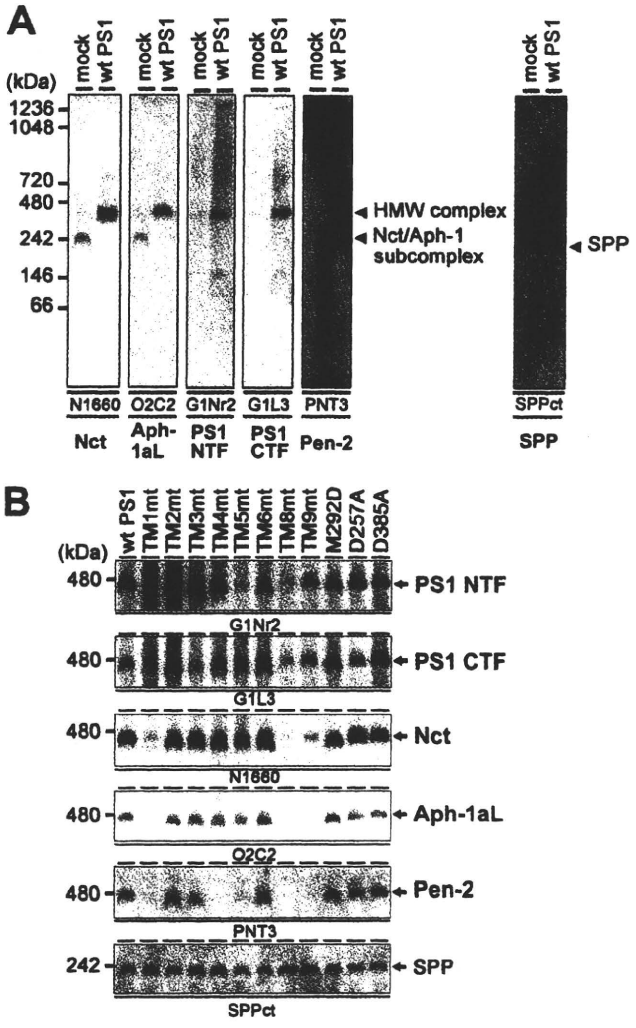

FIGURE 4. **HMW complex formation of TMD-swap PS1 mutants.** *A*, BN-PAGE analysis of digitonin-solubilized lysate prepared from DKO cells expressing mock or WT PS1. Antibodies used as well as target proteins are indicated below the panel. Note that the overexpression of PS1 in DKO cells restored the formation of the HMW complex that migrated at 440 kDa. *B*, BN-PAGE analysis of mutant PS1. SPP was used as loading control as SPP was detected at 200 kDa in this analysis irrespective of PS1 overexpression.

TMD-swap PS1 mutants were almost similar to those of WT PS1, suggesting that the TMD-swap mutations did not cause significant defects in the structural integrity of the PS1 polypeptides. Taken together, these results indicate that the TMD1, -5, -8, and -9 of PS1 are critical regions for the stabilization of the γ-secretase subsequent to the formation of the HMW complex.

Photoaffinity Labeling Experiments Using TMD-swap PS1 Mutants—The biochemical characters of the HMW complex containing the TM2mt or TM6mt PS1 were almost similar to that with WT PS1. To gain further insights into the molecular mechanisms underlying the enzymatic defects of these mutants, we took the photoaffinity labeling approach. The helical peptide-type GSI-based photoprobe pep.11-Bt and the transition state analogue-type GSI-based photoprobe L-852,646 are directly targeted to the initial substrate-binding site and the catalytic site, respectively (5, 6, 21). These probes specifically labeled PS1 NTF as well as PS1/M292D holoprotein, whereas WT PS1 holoprotein was never positively labeled, supporting the notion that the PS1 fragments forming the stabilized HMW complex are the proteolytically active form and that these two distinct functional sites are formed independently of the endoproteolysis (Fig. 7*A*). Moreover, pep.11-Bt bound to the catalytic site mutants (*i.e.* PS1/D257A and PS1/D385A), whereas L-852,646 did not specifically label these catalytic site mutants. Thus, formation of the initial substrate-binding site of γ-secretase appears to take place independently of that of the catalytic site, in agreement with the previous prediction (4). In contrast, TM2mt and TM6mt PS1 were labeled neither by the pep.11-Bt-binding site nor by the L-852,646 catalytic site photoprobes. Photoaffinity labeling experiments combined with intramolecular complementation (*i.e.* co-expression of TM2mt or TM6mt NTF and WT CTF) also resulted in no specific binding of the probes (Fig. 7*B*). These results suggest that TMD2 and the luminal side of TMD6 have critical role(s) in the formation of the initial substrate-binding site and the catalytic site.

TMD2 and -6 Locate in Proximity to TMD9—We have previously reported the functional role of the extracellular/luminal side of PS1 TMD9 in the initial substrate binding of the γ-secretase by SCAM using MTS reagents (9, 11). Of note, a sulfhydryl-based cross-linking experiment revealed that TMD9 locates in proximity to the residue Leu^{250} in TMD6. To test whether TMD2 also locates in proximity to TMD9, we generated mutant PS1 that harbors a single cysteine substituted at residue Ser^{132}, which is placed at the juxtamembrane region of TMD2 on a Cys-less PS1 basis (PS1Cys(−)/S132C). Amino acid substitution of Ser^{132} to cysteine did not affect the γ-secretase activity (Fig. 8*A*). SCAM labeling using *N*-biotinylaminoethyl methanethiosulfonate and competition experiments by charged MTS reagents (*i.e.* negatively charged 2-sulfonato-

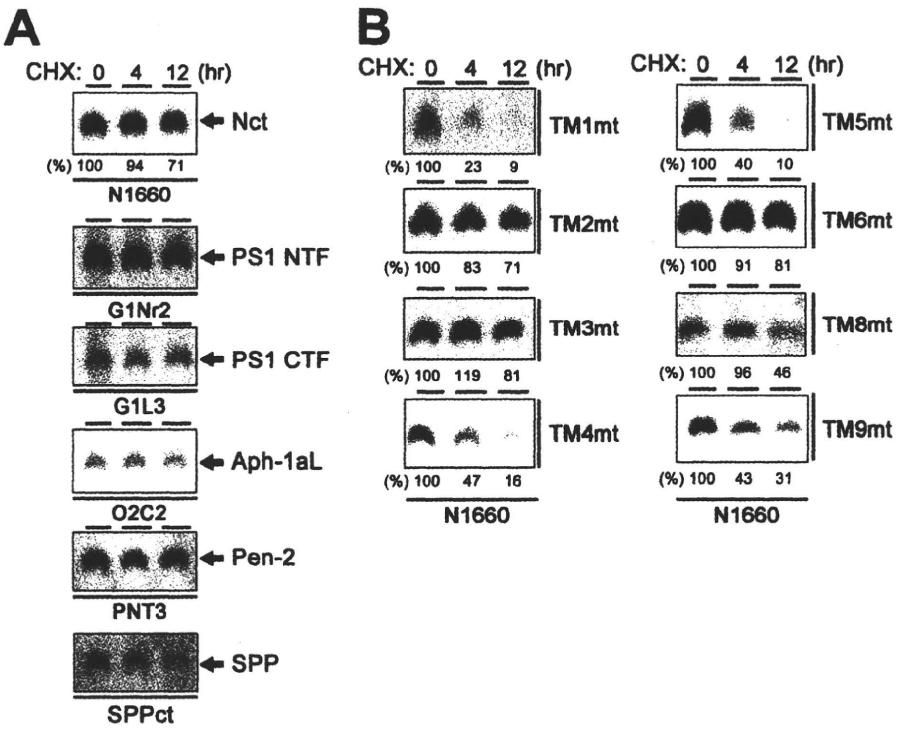

FIGURE 5. **Stability of the HMW complex harboring TMD-swap PS1 mutants.** *A*, analysis of stability of the HMW complex containing WT PS1 in DKO cells incubated in culture medium containing cycloheximide (*CHX*) (30 mg/ml). DKO cells after various incubation periods (0–12 h) were solubilized in BN-PAGE lysis buffer and analyzed by BN-PAGE analysis with each antibody (as indicated below the panel). In immunoblot using anti-Nct antibody, *numbers* shown above or below each lane denote the incubation period and the relative band intensity, respectively. Note that all components were stable over 12 h. *B*, analysis of stability of the HMW complex harboring TMD-swap PS1 mutant probed by anti-Nct antibody.

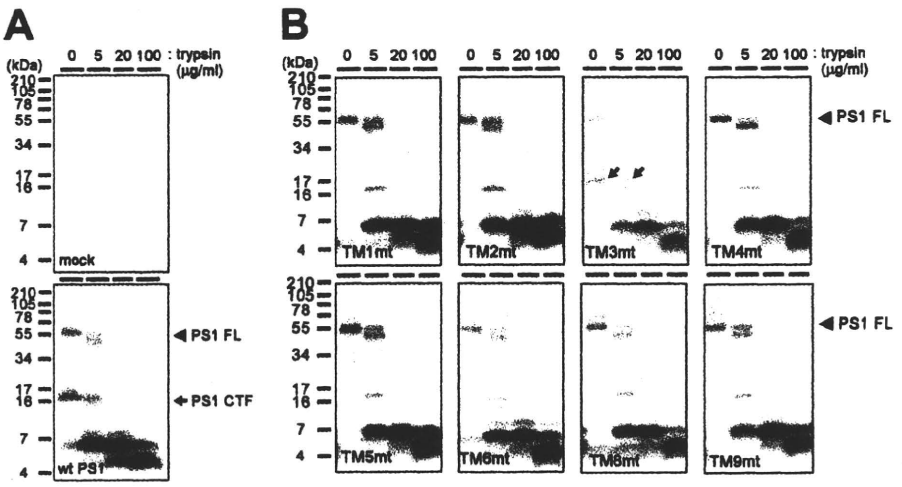

FIGURE 6. **Trypsin digestion of TMD-swap PS1 polypeptides in DKO cells.** 1% CHAPSO-solubilized lysates prepared from DKO cells transiently transfected with WT PS1 (*A*) or TMD-swap PS1 mutants (*B*) were divided into four samples and incubated with trypsin at the indicated concentrations above the panels and analyzed by immunoblotting using the anti-PS1 C terminus antibody (anti-PS-C3). Full-length PS1 (*PS1 FL*) and CTF are shown by *black arrowheads* and *arrows*, respectively. Note that the digestion patterns of mutant PS1 are almost similar, whereas the stability of HMW complex is different (see Fig. 5*B*).

ethyl methanethiosulfonate (*MTSES*) and the bulkier, positively charged 2-(trimethylammonium)-ethyl methanethiosulfonate (*MTSET*) (9, 11)) revealed that Ser^{132} faces an open hydrophilic environment at the extracellular/luminal side (Fig. 8*B*). Next we tested whether S132C was cross-linked with residues Asp^{450} and Gln^{454} replaced with Cys, which are located at TMD9 and are the most C terminal, respectively (Fig. 8*C*). We utilized MTS cross-linkers MTS-4-MTS (*M4M*) and MTS-14-MTS (*M14M*) with spacer moieties of 7.8 and 20.8 Å long, respectively. We found that the N- and C-terminal fragments of PS1Cys(−)/S132C/D450C double mutant are cross-linked. In contrast, no cross-linked product of the fragments of PS1Cys(−)/S132C/Q454C was detected. These data imply that TMD2 is also located in proximity to TMD9 similarly to TMD6. Taken together, we concluded that TMD2, -6, and -9 of PS1 collaborate to form the initial substrate-binding site of the γ-secretase complex.

DISCUSSION

A number of studies have revealed the seminal roles of the TMDs of the γ-secretase components in the assembly of the active complex and acquisition of its proteolytic activity (12, 15, 17, 18, 24, 25, 32, 33). Previously we and others found the requirement of TMD4 in the binding with Pen-2 (12, 33). Here we furthered the extensive analysis of a series of TMD-swap PS1 proteins and examined their ability to form functional γ-secretase complex in PS null background. The replacement of TMD1, -2, -5, -6, -8, or -9 with irrelevant polypeptide abolished the ability to generate Aβ or NICD, whereas these mutants formed the HMW complex with other γ-secretase components (*i.e.* Nct, Aph-1, and Pen-2). Among the mutants, swap of TMD1, -5, -8, or -9 affected the stability of HMW complex, suggesting that the acquisition of stability of the complex is required for the proteolytic activity. Notably, using the photoaffinity labeling approach, we found that the TMD2 and luminal side of TMD6 of PS1 contribute to the formation of the initial substrate-binding site and the catalytic site. Moreover, an intramolecular complementation assay suggested the role of TMD3 in the acquisition of proper γ-secretase activity after endoproteolysis. The predicted scheme of the relationship between the

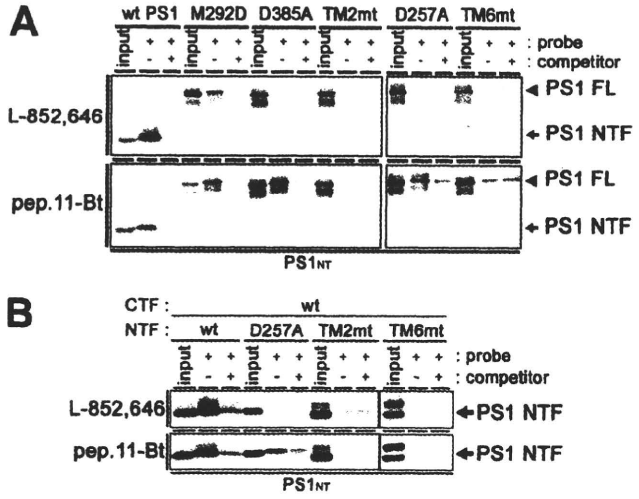

FIGURE 7. **Photoaffinity labeling experiments using TMD-swap PS1 mutants.** *A*, CHAPSO-solubilized DKO cell membranes (DKO cells expressing PS1 holoproteins) were photoactivated in the absence (−) or presence (+) of the parent compound as a competitor and analyzed by immunoblotting with anti-PS1 NTF antibody ($PS1_{NT}$). *PS1 FL*, full-length PS1. *B*, CHAPSO-solubilized DKO cell membranes (DKO cells co-expressing PS1 NTF and PS1 CTF individually from separate vectors) were photoactivated in the absence (−) or presence (+) of the parent compound as a competitor and analyzed by immunoblotting with anti-$PS1_{NT}$ antibody. Probes used are indicated at *left* of the panel.

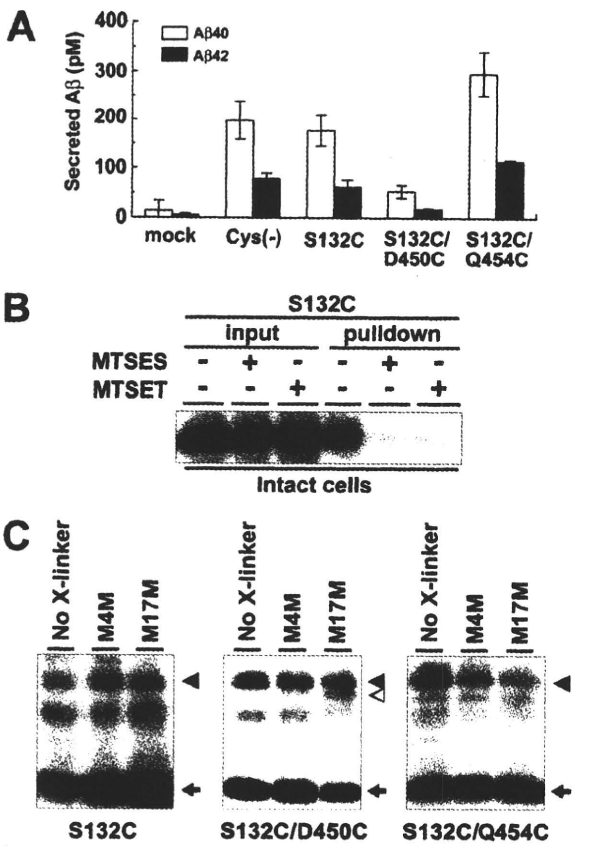

FIGURE 8. **Cross-linking experiment using MTS cross-linkers.** *A*, sandwich ELISA analysis of secreted Aβ from APP_{NL}-stable DKO cells transiently expressing cysteine PS1 mutants. *Error bars* indicate S.E. *B*, SCAM analysis of S132C mutant PS1 using intact cells. *MTSES*, 2-sulfonatoethyl methanethiosulfonate; *MTSET*, 2-(trimethylammonium)-ethyl methanethiosulfonate. *C*, cross-linking experiments of single- (S132C) or double-Cys (S132C/D450C or S132C/Q454C) mutant PS1 in microsomes and immunoblot analysis using anti-$PS1_{NT}$ antibody. Locations of cysteine mutations are shown below the panel. PS1 FL, NTF, and cross-linked product (NTF-CTF heterodimer) are shown by *black arrowheads*, *black arrows*, and *white arrowhead*, respectively. *No X-linker*, no cross-linker; *M4M*, MTS-4-MTS; *M17M*, MTS-17-MTS.

assembly of the γ-secretase and the function of PS1 TMDs is shown in Fig. 9.

Active γ-secretase is known to form a highly stable protein complex (34). Systematic mutational studies of PS support our previous view that the formation of stabilized HMW complex is tightly related to its proteolytic activity (15, 18, 34–36). Nct-Aph-1 subcomplex has been considered as the stabilization factor for the γ-secretase complex (7, 8). In fact, we have recently shown that single chain variable fragment against Nct diminished the stability and activity of the γ-secretase complex (31). However, TM1mt, TM5mt, TM8mt, and TM9mt PS1 failed to be stabilized despite their capability to bind Nct-Aph-1 subcomplex and form the HMW complex. These PS1 mutants recovered complex-type *N*-glycosylated Nct polypeptides that acquired trypsin resistance, indicating that conformational maturation of Nct and the trafficking of the γ-secretase complex occur independently of the stability of PS1. Thus, it is reasonable to conclude that the interaction of PS1 with the Nct-Aph-1 subcomplex is not sufficient for the stability of the γ-secretase. Brunkan *et al.* (36) reported on similar results about TMD1 of PS1. Lack of significant difference in the band patterns of trypsin-digested PS1 mutant polypeptides suggests that the topology of TMDs in the lipid bilayer is not affected by mutagenesis. Instead, these TMDs might contribute to the stabilization as well as structural integrity of PS1 within the functional γ-secretase architecture, which is critical to the enzymatic activity.

Both D257A/PS1 and D385A/PS1 were labeled by pep.11-Bt, but not L-852,646, in the photoaffinity labeling experiments. This is consistent with the previous result that transition state analogue-type and helical peptide-type GSIs target spatially different regions in PS1 and indicates that the formation of the initial substrate-binding site occurs independently of the catalytically active conformation of the γ-secretase complex (4–6). Thus, the result that TM2mt and TM6mt failed to interact with both types of photoprobes suggests that TMD2 and the luminal side of TMD6 are responsible for the formation of the initial substrate-binding site after or during stabilization. In addition, we have found that both TMD2 (this study) and TMD6 (9, 11) are located in proximity to TMD9 within the PS1 CTF. Thus, the former two TMDs might be responsible for the formation of initial substrate-binding site in PS1. However, we cannot fully exclude the possibility that other portions of PS1 are also involved in the substrate binding, and the integrity of these portions was disrupted by conformational changes caused by TMD-swap mutagenesis.

Molecular mechanisms whereby the intramembrane-cleaving enzymes hydrolyze membrane-embedded substrates still remain enigmatic. However, x-ray crystallographic and subsequent biochemical analyses of rhomboid and site-2 proteases, the serine-type and metalloprotease-type intramembrane-cleaving enzymes, respectively, provided some clue to the atypical proteolytic process; initial substrate-enzyme interaction

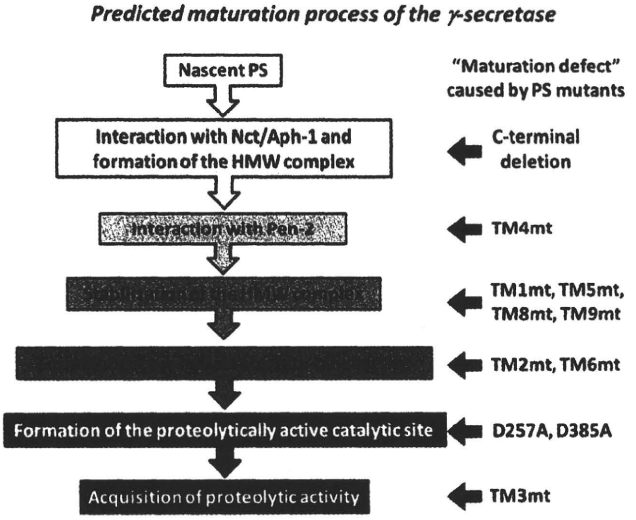

FIGURE 9. **Malfunction of TMD-swap PS1 mutants in the maturation process of the γ-secretase complex.** The maturation process of the γ-secretase complex is indicated as *boxes* with *arrows*. PS1 mutants are indicated at *right* of the process that is defective in the mutant.

should occur via helix-helix interface in a hydrophobic environment (37). Then the substrate is transferred into the hydrophilic catalytic pore through the lateral gate. TMD9 of PS1 is implicated in the substrate binding and the gating mechanism, whereas structural information regarding PS1 at higher resolution has been lacking. Of note, using recombinant protein-based binding assay, a region containing PS1 TMD2 is implicated in the direct substrate binding (38). In regard to TMD6, we have shown that the luminal side of TMD6 is exposed to a hydrophilic environment along with the catalytic aspartate residue, Asp^{257}, by SCAM (9, 10). Pharmacological and chemical biological analyses have indicated that the initial substrate binding and the catalytic sites are located in proximity (5, 6). Thus, the luminal side of TMD6 might be one of the structural constituents not only of the catalytic site but also of the initial substrate-binding site. The luminal half of TMD6 has been shown to comprise an α-helical structure, of which one plane formed by residues Ala^{246}, Leu^{250}, and Asp^{257} is exposed to the hydrophilic milieu of the catalytic pore (9). We propose that the reverse side of this segment that faces the lipid bilayer might comprise the initial substrate-binding interface. Binding of the substrate to the initial binding site composed of TMD2, -6, and -9 may induce a conformational change of PS1 and facilitate the access of the substrate to the catalytic site. A similar substrate-binding and catalytic site relationship has been reported in the rhomboid (39).

In sum, we have revealed that PS1 TMD1, -5, -8, and -9 are required for the stabilization of the HMW complex and that TMD2 and the luminal side of TMD6 contribute to the formation of the initial substrate-binding site of the γ-secretase. However, we cannot fully exclude the possibility that the TMD swapping might alter the overall conformation of the presenilin polypeptide in a way that could alter its function. Additional mutagenesis studies will be needed to further identify the critical domains in PS1 for the substrate recognition. X-ray crystallographic analyses would eventually reveal the mechanism by which the γ-secretase complex recognizes the substrate and the substrate enters the active site.

Acknowledgments—We thank Drs. B. De Strooper (Katholieke Universiteit Leuven, Leuven, Belgium), R. Kopan (Washington University in St. Louis, St. Louis, MO), T. Kitamura (The University of Tokyo, Tokyo, Japan), Y. M. Li (Sloan Kettering Cancer Center, New York, NY), G. Thinakaran (The University of Chicago, Chicago, IL), A. Takashima (RIKEN, Saitama, Japan), and T. E. Golde (Mayo Clinic, Jacksonville, FL) for valuable reagents, Takeda Pharmaceutical Company (Osaka, Japan) for Aβ ELISA, and our current/previous laboratory members for helpful discussions and technical assistance.

REFERENCES

1. Tomita, T. (2009) *Expert Rev. Neurother.* **9,** 661–679
2. Wolfe, M. S. (2009) *Semin. Cell Dev. Biol.* **20,** 219–224
3. Takasugi, N., Tomita, T., Hayashi, I., Tsuruoka, M., Niimura, M., Takahashi, Y., Thinakaran, G., and Iwatsubo, T. (2003) *Nature* **422,** 438–441
4. Esler, W. P., Kimberly, W. T., Ostaszewski, B. L., Ye, W., Diehl, T. S., Selkoe, D. J., and Wolfe, M. S. (2002) *Proc. Natl. Acad. Sci. U.S.A.* **99,** 2720–2725
5. Kornilova, A. Y., Bihel, F., Das, C., and Wolfe, M. S. (2005) *Proc. Natl. Acad. Sci. U.S.A.* **102,** 3230–3235
6. Imamura, Y., Watanabe, N., Umezawa, N., Iwatsubo, T., Kato, N., Tomita, T., and Higuchi, T. (2009) *J. Am. Chem. Soc.* **131,** 7353–7359
7. LaVoie, M. J., Fraering, P. C., Ostaszewski, B. L., Ye, W., Kimberly, W. T., Wolfe, M. S., and Selkoe, D. J. (2003) *J. Biol. Chem.* **278,** 37213–37222
8. Niimura, M., Isoo, N., Takasugi, N., Tsuruoka, M., Ui-Tei, K., Saigo, K., Morohashi, Y., Tomita, T., and Iwatsubo, T. (2005) *J. Biol. Chem.* **280,** 12967–12975
9. Sato, C., Morohashi, Y., Tomita, T., and Iwatsubo, T. (2006) *J. Neurosci.* **26,** 12081–12088
10. Tolia, A., Chávez-Gutiérrez, L., and De Strooper, B. (2006) *J. Biol. Chem.* **281,** 27633–27642
11. Sato, C., Takagi, S., Tomita, T., and Iwatsubo, T. (2008) *J. Neurosci.* **28,** 6264–6271
12. Watanabe, N., Tomita, T., Sato, C., Kitamura, T., Morohashi, Y., and Iwatsubo, T. (2005) *J. Biol. Chem.* **280,** 41967–41975
13. Kitamura, T., Koshino, Y., Shibata, F., Oki, T., Nakajima, H., Nosaka, T., and Kumagai, H. (2003) *Exp. Hematol.* **31,** 1007–1014
14. Morohashi, Y., Kan, T., Tominari, Y., Fuwa, H., Okamura, Y., Watanabe, N., Sato, C., Natsugari, H., Fukuyama, T., Iwatsubo, T., and Tomita, T. (2006) *J. Biol. Chem.* **281,** 14670–14676
15. Tomita, T., Takikawa, R., Koyama, A., Morohashi, Y., Takasugi, N., Saido, T. C., Maruyama, K., and Iwatsubo, T. (1999) *J. Neurosci.* **19,** 10627–10634
16. Morohashi, Y., Hatano, N., Ohya, S., Takikawa, R., Watabiki, T., Takasugi, N., Imaizumi, Y., Tomita, T., and Iwatsubo, T. (2002) *J. Biol. Chem.* **277,** 14965–14975
17. Leem, J. Y., Saura, C. A., Pietrzik, C., Christianson, J., Wanamaker, C., King, L. T., Veselits, M. L., Tomita, T., Gasparini, L., Iwatsubo, T., Xu, H., Green, W. N., Koo, E. H., and Thinakaran, G. (2002) *Neurobiol. Dis.* **11,** 64–82
18. Saura, C. A., Tomita, T., Soriano, S., Takahashi, M., Leem, J. Y., Honda, T., Koo, E. H., Iwatsubo, T., and Thinakaran, G. (2000) *J. Biol. Chem.* **275,** 17136–17142
19. Nyborg, A. C., Kornilova, A. Y., Jansen, K., Ladd, T. B., Wolfe, M. S., and Golde, T. E. (2004) *J. Biol. Chem.* **279,** 15153–15160
20. Tomita, T., Maruyama, K., Saido, T. C., Kume, H., Shinozaki, K., Tokuhiro, S., Capell, A., Walter, J., Grünberg, J., Haass, C., Iwatsubo, T., and Obata, K. (1997) *Proc. Natl. Acad. Sci. U.S.A.* **94,** 2025–2030
21. Li, Y. M., Xu, M., Lai, M. T., Huang, Q., Castro, J. L., DiMuzio-Mower, J., Harrison, T., Lellis, C., Nadin, A., Neduvelil, J. G., Register, R. B., Sardana, M. K., Shearman, M. S., Smith, A. L., Shi, X. P., Yin, K. C., Shafer, J. A., and Gardell, S. J. (2000) *Nature* **405,** 689–694
22. Fuwa, H., Takahashi, Y., Konno, Y., Watanabe, N., Miyashita, H., Sasaki,